Distinct disease-specific Tfh cell populations in 2 different fibrotic diseases:IgG4-related disease and Kimura disease

宗村, 龍祐

Distinct disease-specific Tfh cell populations in 2 different fibrotic diseases: IgG$_4$-related disease and Kimura disease

Ryusuke Munemura, DDS,[a] Takashi Maehara, DDS, PhD,[a,j] Yuka Murakami, DDS,[a] Risako Koga, DDS,[a] Ryuichi Aoyagi, DDS,[a] Naoki Kaneko, DDS, PhD,[a] Atsushi Doi, PhD,[b] Cory A. Perugino, DO,[c,d] Emanuel Della-Torre, MD,[e] Takako Saeki, MD,[f] Yasuharu Sato, DDS, PhD,[g] Hidetaka Yamamoto, MD, PhD,[h] Tamotsu Kiyoshima, DDS, PhD,[i] John H. Stone, MD, MPH,[c] Shiv Pillai, MBBS, PhD,[d] and Seiji Nakamura, DDS, PhD[a] *Fukuoka, Nagaoka, and Okayama, Japan; Boston, Mass; and Milan, Italy*

GRAPHICAL ABSTRACT

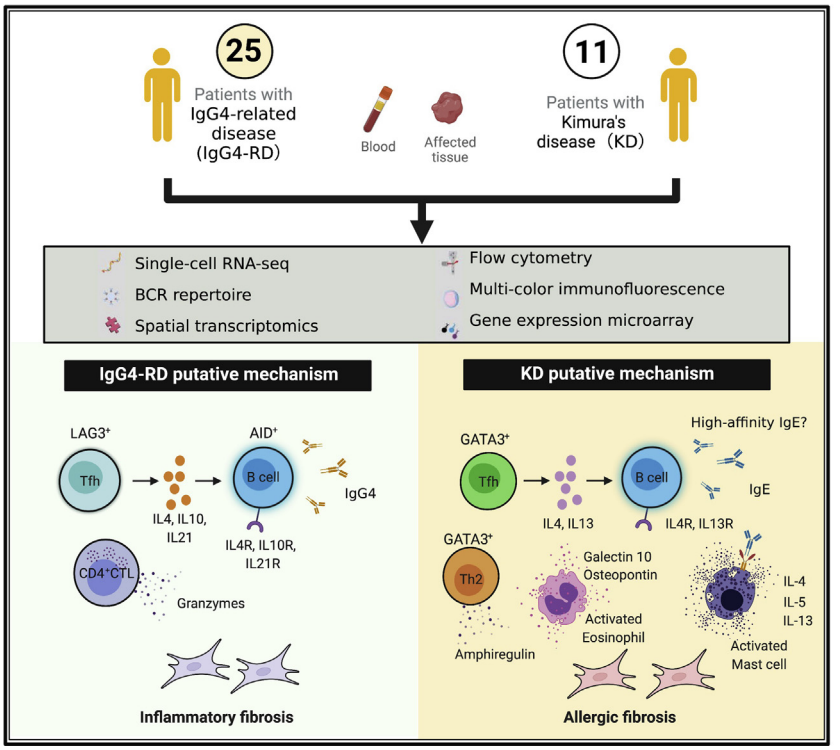

From [a]the Section of Oral and Maxillofacial Oncology, Division of Maxillofacial Diagnostic and Surgical Sciences, Faculty of Dental Science, Kyushu University, Fukuoka; [b]Cell Innovator Inc, Fukuoka; [c]the Division of Rheumatology, Allergy, and Immunology, Massachusetts General Hospital, Harvard Medical School, Boston; [d]the Ragon Institute of MGH, MIT, and Harvard, Massachusetts General Hospital, Harvard Medical School, Boston; [e]the Unit of Immunology, Rheumatology, Allergy, and Rare Diseases, IRCCS San Raffaele Scientific Institute, Milan; [f]the Department of Internal Medicine, Nagaoka Red Cross Hospital, Nagaoka; [g]the Okayama University Graduate School of Medicine, Dentistry, and Pharmaceutical Sciences, Okayama; [h]the Division of Diagnostic Pathology, Kyushu University Hospital, Fukuoka; [i]the Laboratory of Oral Pathology, Division of Maxillofacial Diagnostic and Surgical Sciences, Faculty of Dental Science, Kyushu University, Fukuoka; and [j]the Dento-craniofacial Development and Regeneration Research Center, Faculty of Dental Science, Kyushu University, Fukuoka.

The first 2 authors contributed equally to this article, and both should be considered first author.

This study was supported by Japan Society for the Promotion of Science (JSPS) Grants-in-Aid for Scientific Research (KAKENHI) (grants JP18KK0260, 21K19607, and JP19H03854), the Kanae Foundation for the Promotion of Medical Science, the R3QR program (Qdai-jump research program 01216), and the Takeda Science Foundation) (all to T.M.) and by JSPS KAKENHI grant JP20H00553 (to S.N.). S.P. was supported by National Institutes of Health grant U19 AI110495. C.A.P. was supported by a Rheumatology Research Foundation Scientist Development Award.

Disclosure of potential conflict of interest: The authors declare that they have no relevant conflicts of interest.

Received for publication December 18, 2021; revised March 1, 2022; accepted for publication March 21, 2022.

Available online May 11, 2022.

Corresponding author: Takashi Maehara, DDS, PhD, Section of Oral and Maxillofacial Oncology, Division of Maxillofacial Diagnostic and Surgical Sciences, Faculty of Dental Science, Kyushu University, Fukuoka, Japan. E-mail: tmaehara@dent.kyushu-u.ac.jp.

0091-6749/$36.00

https://doi.org/10.1016/j.jaci.2022.03.034

Background: How T follicular (Tfh) cells contribute to many different B-cell class-switching events during T-cell–dependent immune responses has been unclear. Diseases with polarized isotype switching offer a unique opportunity for the exploration of Tfh subsets. Secondary and tertiary lymphoid organs in patients with elevated tissue expression levels of IgE (Kimura disease, KD) and those of IgG_4 (IgG_4-related disease, IgG_4-RD) can provide important insights regarding cytokine expression by Tfh cells.

Objective: We sought to identify disease-specific Tfh cell subsets in secondary and tertiary lymphoid organs expressing IL-10 or IL-13 and thus identify different cellular drivers of class switching in 2 distinct types of fibrotic disorders: allergic fibrosis (driven by type 2 immune cells) and inflammatory fibrosis (driven by cytotoxic T lymphocytes).

Methods: Single-cell RNA sequencing, *in situ* sequencing, and multicolor immunofluorescence analysis were used to investigate B cells, Tfh cells, and infiltrating type 2 cells in lesion tissues from patients with KD or IgG_4-RD.

Results: Infiltrating Tfh cells in tertiary lymphoid organs from IgG_4-RD were divided into 6 main clusters. We encountered abundant infiltrating *IL-10*–expressing *LAG3*$^+$ Tfh cells in patients with IgG_4-RD. Furthermore, we found that infiltrating *AICDA*$^+$*CD19*$^+$ B cells expressing *IL-4*, *IL-10*, and *IL-21* receptors correlated with IgG_4 expression. In contrast, we found that infiltrating IL-13–expressing Tfh cells were abundant in affected tissues from patients with KD. Moreover, we observed few infiltrating IL-13–expressing Tfh cells in tissues from patients with IgG_4-RD, despite high serum levels of IgE (but low IgE in the disease lesions). Cytotoxic T cells were abundant in IgG_4-RD; in contrast, type 2 immune cells were abundant in KD.

Conclusions: Our analysis revealed a novel subset of *IL-10*$^+$*LAG3*$^+$ Tfh cells infiltrating the affected organs of IgG_4-RD patients. In contrast, IL-13$^+$ Tfh cells and type 2 immune cells infiltrated those of KD patients. (J Allergy Clin Immunol 2022;150:440-55.)

Key words: *Single-cell RNA sequencing, IgG_4-related disease, IgG_4-RD, IgG_4, IgE, Tfh cell, B cell, interleukin-10, class switch, fibrosis*

Abbreviations used

CS:	Chronic sialoadenitis
cTfh:	Circulating Tfh
CTL:	Cytotoxic T lymphocyte
DAPI:	4′,6-Diamidino-2-phenylindole
IgG_4-RD:	IgG_4-related disease
ILC2:	Type 2 innate lymphoid cell
KD:	Kimura disease
OPN:	Osteopontin
scRNA-Seq:	Single-cell RNA sequencing
SjS:	Sjögren syndrome
SLO:	Secondary lymphoid organ
Tfh:	T follicular
Tfh13:	IL-13–secreting Tfh
Tfr:	Regulatory follicular helper T
TLO:	Tertiary lymphoid organ
t-SNE:	*t*-Distributed stochastic neighbor embedding

T follicular (Tfh) cells are a subset of CD4$^+$ T cells that assist B cells during T-cell–dependent immune responses and contribute to isotype switching, somatic hypermutation, germinal center formation, and high-affinity B-cell selection in germinal centers.[1,2] Tfh cells are distinguished from other CD4$^+$ T cells on the basis of their expression of ICOS and Bcl6. Tfh cells were originally observed in the light zones of germinal centers, but broadly similar cells have also been observed outside follicles at the T-cell zone–B-cell follicle interface, known as the T-B interface. While some studies have referred to these broadly similar cells as Tfh cells, this is not universally accepted, as these cells reside outside the follicle; they have also been referred to as pregerminal center Tfh cells.[3] We and other groups have argued that class-switching events also occur outside the follicle.[4,5] Nevertheless, how Tfh cells or Tfh-like cells contribute to class-switching events at more than 1 location remains unclear.

IgG_4-related disease (IgG_4-RD) is a fibrotic, systemic, inflammatory disease of unknown etiology.[6] The expansion of circulating plasmablasts, most of which express IgG_4, is a hallmark of active IgG_4-RD.[7] These blood plasmablasts are heavily somatically hypermutated, implying that they may be derived from germinal centers with assistance from Tfh cells. Histologic analyses have shown that ectopic germinal centers frequently occur in affected salivary glands in patients with IgG_4-RD.[8] IgG_4-RD is a disease that involves polarized class switching to IgG_4, but many patients also have elevated serum levels of IgG_1, IgE, or both.[6] Notably, patients with nonallergic disease who have IgG_4-RD also show elevated serum IgE.[9] Although the mechanisms underlying the switch to IgG_4 in IgG_4-RD are poorly understood, IL-10 is presumed to indirectly contribute to IgG_4 class switching by facilitating IL-4–mediated switching to IgG_4, rather than to IgE.[10] Our previous multicolor immunofluorescence analysis revealed that IL-4$^+$ Tfh cells were expanded in patients with IgG_4-RD.[5] However, our previous studies were not performed at the single-cell level. Furthermore, Tfh cells expressing other cytokines have not been investigated in secondary lymphoid organs (SLOs) and tertiary lymphoid organs (TLOs) from IgG_4-RD patients.

Kimura disease (KD) is a rare, chronic inflammatory disorder that is characterized by subcutaneous eosinophilic lymph follicular granuloma in affected tissues and high serum IgE levels. Other similar manifestations have been observed in KD and IgG_4-RD. Ectopic germinal center formation,[11] infiltrating tissue eosinophilia, peripheral eosinophilia, or high serum IgE levels are often found in IgG_4-RD patients, especially among those with manifestations such as sialoadenitis, dacryoadenitis, and orbital disease. From these clinicopathologic observations, T_H2 cells and allergic triggers were once hypothesized to be important in the pathogenesis of both diseases, although there is little evidence for T_H2 cells accumulating in tissues in IgG_4-RD.[8,9,12,13] Gowthaman et al[14] showed that IL-4$^+$ Tfh cells induce direct switching of B cells to low-affinity IgE during a subset of type 2 immune responses, but IL-13–secreting Tfh (Tfh13) cells produce additional signals that regulate high-affinity IgE during allergic responses. Tfh13 cells are distinguished by their cytokine products (eg, IL-4, IL-5, and IL-13) and expression of GATA3. Tfh13 cells were found within germinal centers in mice and were also expanded in blood from human patients with allergies.[14]

Both KD and IgG_4-RD lesions are characterized by fibrosis.[6,11] Fibrosis is the end result of chronic inflammatory reactions induced by various stimuli including persistent infections, autoimmune reactions, allergic responses, radiation, and tissue injury. Fibrotic diseases likely have many different etiologies, and they may not all be driven by $CD4^+$ T cells. In our previous study examining the etiology of tissue fibrosis in patients with IgG_4-RD, we found that recurrent apoptotic cell death, driven by the recognition of self-peptides by autoreactive $CD4^+$ cytotoxic T lymphocyte (CTL) and $CD8^+$ CTL clones, may contribute to cell loss and subsequent extensive tissue remodeling, leading to fibrosis and organ dysfunction.[15] In contrast, type 2 immune cells and their cytokines (IL-4, IL-5, and IL-13) are critical in the pathogenesis of allergic inflammation and fibrosis.[16] Type 2 immunity induces a complex inflammatory response characterized by eosinophils, mast cells, basophils, type 2 innate lymphoid cells (ILC2s), T_H2 cells, and specific IgE antibody subclasses that are crucial to the pathogenesis of many allergic and fibrotic disorders.

This study investigated 2 chronic human diseases with polarized isotype switching to obtain insights regarding unique Tfh cell subsets. We found that SLOs and TLOs in patients with elevated tissue expression levels of IgE and IgG_4 represent useful substrates for examining distinct cytokine expression by Tfh cells and Tfh-like cells in the context of KD and IgG_4-RD. We also identified distinct disease-specific Tfh cell subsets expressing IL-10 in IgG_4-RD patients. Furthermore, we characterized differences in the etiologies of inflammatory and allergic fibrosis and identified 2 different types of fibrosis: allergic fibrosis (driven by type 2 cells) and inflammatory fibrosis (driven by cytotoxic T cells).

METHODS

This study included 11 KD patients, 25 IgG_4-RD patients, 16 Sjögren syndrome (SjS) patients, and 10 chronic sialoadenitis (CS) patients. CS is a nonspecific inflammatory disease of the salivary glands linked to sialolithiasis. Patients were followed up between 2010 and 2021 at the Department of Oral and Maxillofacial Surgery of Kyushu University Hospital, a tertiary-care center. Open submandibular gland biopsy samples were obtained from IgG_4-RD patients, while CS patients underwent submandibulectomy. Lip biopsy samples were obtained from SjS patients. IgG_4-RD was diagnosed according to previously established criteria.[17] SjS was diagnosed as previously described.[18] Each patient exhibited objective evidence of salivary gland involvement that was based on the presence of subjective xerostomia and a decreased saliva flow rate, abnormal findings on parotid sialography, and focal lymphocytic infiltrates in labial salivary glands. None of the patients had a history of treatment with steroids or other immunosuppressants, or infection with human immunodeficiency virus, hepatitis B virus, or hepatitis C virus; no patient had sarcoidosis or evidence of lymphoma at the time of the study. All patients had strong lymphocytic infiltration in these tissues.

The study protocol was approved by the institutional review board of the Center for Clinical and Translational Research of Kyushu University Hospital (approval 834-00) and followed the tenets of the Declaration of Helsinki. All participants provided written informed consent.

Infiltrating immune cells and sorted $CD3^+$ T cells and $CD19^+$ B cells from 4 IgG_4-RD patients were used for single-cell RNA sequencing (scRNA-Seq). Experimental procedures for scRNA-Seq followed established techniques using the Chromium Single Cell 5′ Library V2 kit (10× Genomics, Pleasanton, Calif). To obtain the T-cell and B-cell receptor repertoire profile from 3 IgG_4-RD patients, V(D)J enrichment for B-cell receptors was carried out with the Chromium Single Cell V(D)J Enrichment Human T Cell kit (10× Genomics). Paraffin-embedded salivary gland sections from 21 IgG_4-RD patients and 11 KD patients were used for multicolor immunofluorescence staining, performed as previously described.[5] Images of tissue specimens were acquired using the TissueFAXS platform (TissueGnostics, Studio City, Calif). Cells of a particular phenotype were identified and quantified by TissueQuest software (TissueGnostics).[19] More details are provided in the Methods section in this article's Online Repository available at www.jacionline.org.

RESULTS

B cells activated to switch to IgG_4 are prominent in affected lesions from IgG_4-RD patients, whereas IgE^+ B cells are prominent in KD

Serum IgG_4 and IgG levels were higher in IgG_4-RD patients than in KD patients. KD patients exhibited an elevated eosinophil count and elevated IgE concentration (see Tables E1–E3 in the Online Repository at www.jacionline.org). Ectopic germinal centers were frequently observed in affected tissue sites in IgG_4-RD and KD patients but were absent or sparse in SjS and CS patients (Fig 1, *A,* and see Table E4 in the Online Repository at www.jacionline.org). We next analyzed SLOs and affected TLOs from KD patients and IgG_4-RD patients. TLOs with germinal centers[20] were identified by multicolor immunofluorescence approaches (CD4, CD19, Bcl6, and 4′,6-diamidino-2-phenylindole [DAPI] expression), and ectopic germinal centers were also identified using multicolor immunofluorescence approaches (CD19, CXCR5, and Bcl6 expression) (Fig 1, *B*). We found that 7 (63.6%) of 11 KD patients, 18 (72%) of 25 IgG_4-RD patients, and 2 (11.8%) of 17 SjS patients had ectopic germinal centers in affected lesions (Table E4). High frequencies and numbers of ectopic germinal centers were observed in affected lesions of KD patients and IgG_4-RD patients.

Germinal center reaction is a multistep process during which naive B cells become immunoglobulin-producing cells. We thus analyzed tissue-infiltrating, immunoglobulin-producing B cells in TLOs from KD patients and IgG_4-RD patients. IgE-positive cells were mainly localized in interfollicular areas in TLOs from KD patients (Fig 1, *C*). IgE was expressed either on the plasma membrane or in the cytoplasm. In KD patients, substantial numbers of IgE-positive cells were detected in and around germinal centers; however, these cells were absent or sparse in IgG_4-RD patients. In contrast, IgG_4-positive cells were abundant in IgG_4-RD patients but not in KD patients.

We next analyzed draining lymph nodes from KD patients and IgG_4-RD patients to evaluate B-cell class switching to IgE and/or IgG_4. Lymph nodes were stained using antibodies to IgE, IgG_4, and CD19 and DAPI as a nuclear stain (Fig 1, *D*). IgE^+CD19^+ B cells represented less than 5% of all $CD19^+$ B cells in normal tonsils from healthy controls and lymph nodes from IgG_4-RD patients. In contrast, IgE^+CD19^+ B cells comprised approximately 30% of $CD19^+$ B cells in KD patients. Furthermore, $IgG_4{}^+CD19^+$ B cells represented less than 6% of all $CD19^+$ B cells in normal tonsils from healthy controls and lymph nodes from KD patients. In contrast, $IgG_4{}^+CD19^+$ B cells comprised approximately 40% of $CD19^+$ B cells in IgG_4-RD patients.

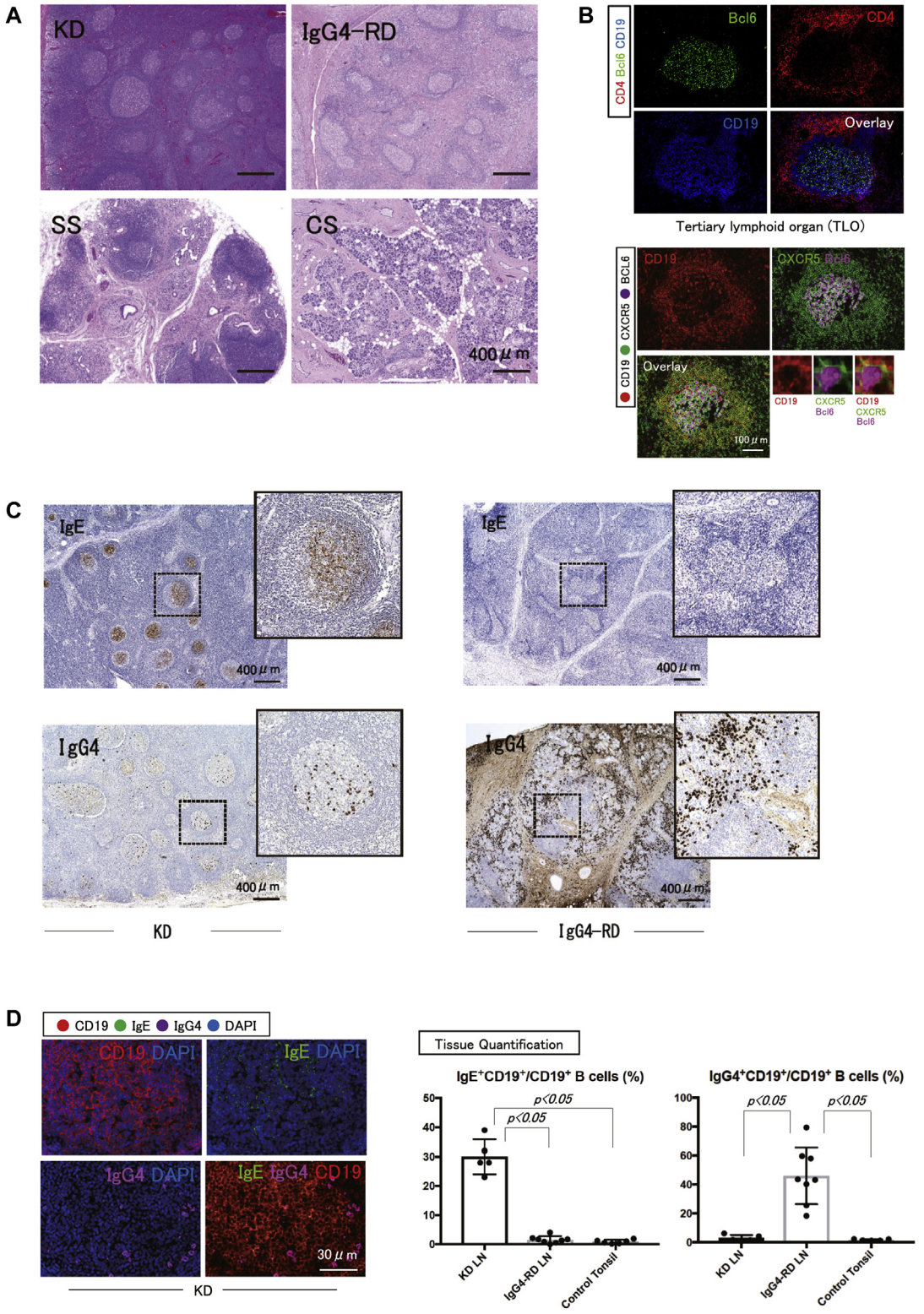

FIG 1. B cells express IgG_4 in affected lesions from patients with IgG_4-RD, in contrast to IgE-expressing B cells in patients with KD. **A,** Ectopic germinal center formation in salivary gland sections from patients with KD, IgG_4-RD, SjS, and CS. **B,** *Top,* Multicolor immunofluorescence staining of CD4 (*red*), Bcl6 (*green*), and CD19 (*blue*) in a TLO from a patient with KD. *Bottom,* Multicolor immunofluorescence staining for CD19 (*red*), CXCR5 (*green*), and Bcl6 (*magenta*) in ectopic germinal centers of salivary glands from a patient with KD. **C,** Immunostaining with IgE and IgG_4 monoclonal antibodies in affected salivary glands from a patient with KD and a patient with IgG_4-RD. **D,** Multicolor immunofluorescence staining of CD19 (*red*), IgE (*green*), IgG_4 (*magenta*), and DAPI (*blue*) in a draining lymph node from a patient with KD. Quantification of IgE^+CD19^+ B cells and $IgG_4^+CD19^+$ B cells in draining lymph nodes from 5 patients with KD, 8 patients with IgG_4-RD, and 6 control tonsils. *P* value was determined by Mann-Whitney *U* test.

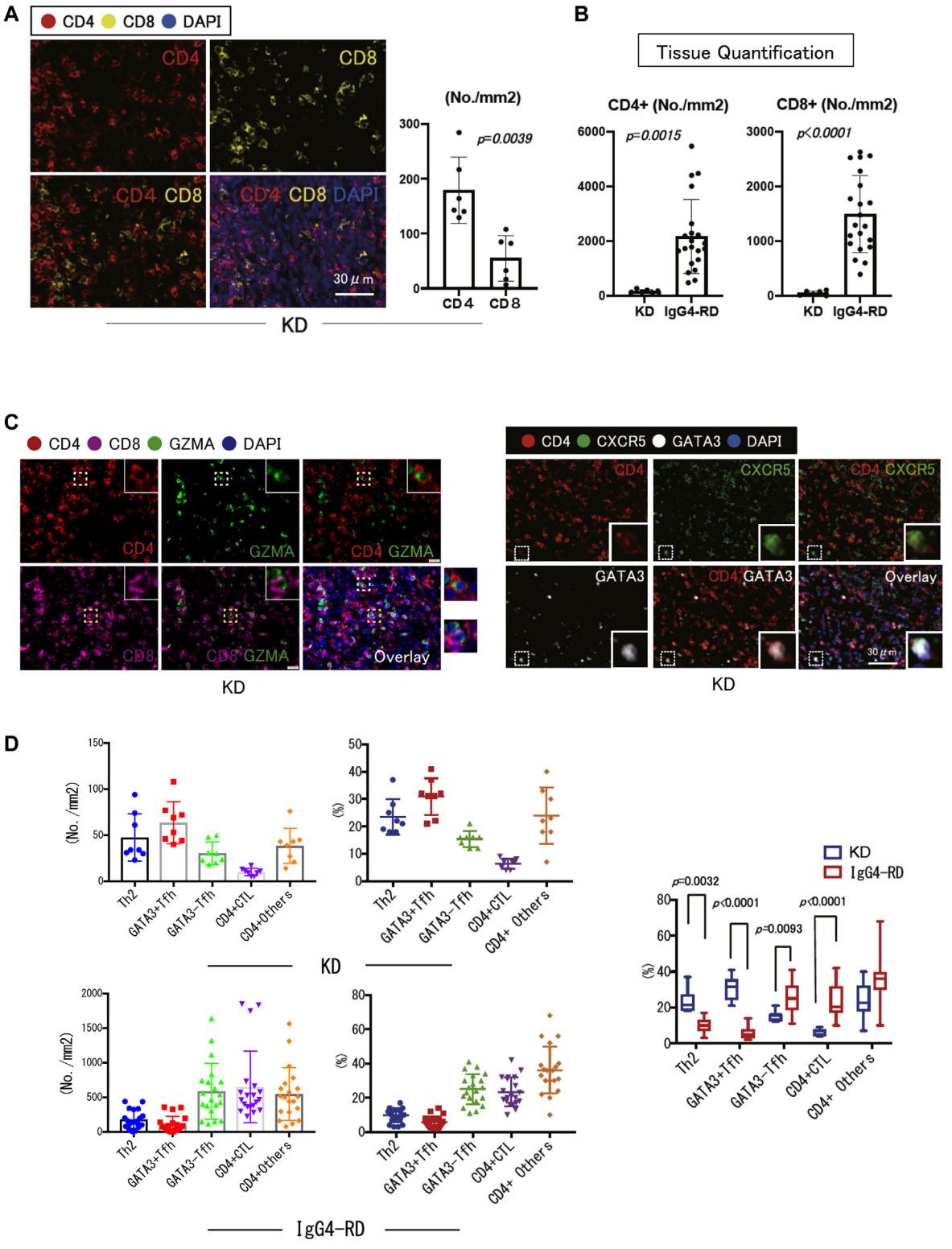

FIG 2. Quantification of $CD4^+$ T cell subsets in patients with KD and patients with IgG_4-RD. **A,** Immunofluorescence staining of CD4 (*red*) and CD8 (*yellow*) T cells and absolute numbers of $CD4^+$ T cells and $CD8^+$ T cells per square millimeter in affected lesions from 6 patients with KD. *P* value was determined by Student *t* test. **B,** Absolute numbers of $CD4^+$ T cells and $CD8^+$ T cells per square millimeter in affected tissues from patients with KD (n = 6) and patients with IgG_4-RD (n = 20). *P* value was determined by Student *t* test. **C,** *Left,* Immunofluorescence staining of CD4 (*red*), CD8 (*magenta*), GZMA (*green*), and DAPI (*blue*) in affected tissues from patients with KD. Quantification of $CD4^+GZMA^+$ CTLs in affected tissues from patients with KD (n = 6) and IgG_4-RD (n = 21). *P* value was determined by Student *t* test. *Right,* Immunofluorescence staining of CD4 (*red*), CXCR5 (*green*), GATA3 (*white*), and DAPI (*blue*) in affected tissue from a patient with KD.

Overall, elevated serum IgG_4 levels and numbers of IgG_4-positive B cells in germinal centers were observed in IgG_4-RD patients, suggesting that B cells may have been activated by disease-specific Tfh cells. Class switching is linked to Tfh cells in SLOs and TLOs and not to other tissue-infiltrating $CD4^+$ T-cell subsets.

$CD4^+CXCR5^+$ Tfh cells are located near $AICDA^+$ B cells

AICDA, also known as AID, encodes an enzyme with roles in class switching, recombination, and somatic hypermutation. To assess spatial gene expression in $AICDA^+CD19^+$ B cells in affected lesions, we performed spatial transcriptomics analysis (10× Genomics) of tissue sections from a patient with IgG_4-RD. Transcriptomes from 1914 spots in a single section were obtained, yielding a median of 2722 genes per spot (see Fig E1, *A,* in the Online Repository at www.jacionline.org). These 1914 spots were divided into 7 cluster types using *t*-distributed stochastic neighbor embedding (t-SNE) visualization (Fig E1, *A*). One spot included approximately 6 to 10 cells. We initially focused on $AICDA^+CD19^+$ B-cell cluster spots. As shown in Fig E1, *B,* cells in cluster 6 expressed high levels of *SERPINA9, KLHL6, BIK, CD22, RGS13, LRMP,* and *ELL3;* these genes were coexpressed with *AICDA*. Cells in cluster 6 also expressed high levels of *CD4, CXCR5, PDCD1, Bcl6, CD40,* and *CXCL13;* these genes are characteristic of Tfh cells. Notably, $CD4^+CXCR5^+$ Tfh cell spots were located near $AICDA^+$ B-cell spots.

Potential recruitment mechanisms for infiltrating Tfh and B cells were also assessed by analyzing chemokine and receptor expression by spatial transcriptomics (Fig E1, *C*). At the T-cell zone–B cell follicle interface, transcripts linked to *CXCL13-CXCR5* signaling were upregulated in cluster 6, suggesting the induction of the migration of Tfh cells into the follicle. At this T-B interface in cluster 6, significant upregulation of genes involved in T- and B-cell receptor signaling pathway was observed (Fig E1, *D*).

As shown in Fig E1, *E,* AID-expressing B cells were visualized both inside and outside germinal centers in IgG-RD sections. Furthermore, T cells expressing ICOS (a marker of Tfh cells) were physically close to AID-expressing B cells in IgG_4-RD TLOs.

GATA3-expressing $CD4^+CXCR5^+$ Tfh-like and T_H2 cells are prominent in KD tissues, while GATA3-negative $CD4^+CXCR5^+$ Tfh-like and $CD4^+$ cytotoxic T cells are prominent in IgG_4-RD tissues

T cells are implicated in the pathogenesis of KD, IgG_4-RD, and other immune-related diseases for multiple reasons and primarily because many $CD4^+$ T cells are present in affected tissues (Fig 2, *A*). To explore the relevance of T and B cells in the pathogenesis of KD and IgG_4-RD, we quantified $CD3^+$ T-cell subsets in affected lesions from KD and IgG_4-RD patients (Fig 2, *B*). We previously found that IgG_4-RD patients had expanded infiltrating $CD4^+GZMA^+$ CTLs in affected lesions.[21] We observed a striking dominance of $CD4^+GZMA^+$ CTLs in affected lesions from IgG_4-RD patients; however, these CTLs were sparse in affected lesions from KD patients (Fig 2, *C*). Although other $CD4^+$ T-cell subsets have been implicated in the pathogenesis of KD, to our knowledge, comprehensive tissue quantitative approaches have not been previously reported. We therefore quantified all major $CD4^+$ T-cell subsets, including T_H1, T_H2, T_H17, and Tfh cells, as well as Treg cells and $CD4^+$ CTLs. Most T cells in KD patients were T_H2 and Tfh cells (see Fig E2 in the Online Repository at www.jacionline.org). GATA3-expressing $CD4^+CXCR5^+$ Tfh cells were abundant in tissue lesions of KD patients but were sparse in IgG_4-RD (Fig 2, *D*). In contrast, $CD4^+$ CTLs and GATA3− Tfh cells were abundant in tissue lesions of IgG_4-RD patients. GATA3-expressing Tfh cells might therefore represent important disease-related type 2 Tfh cells in KD patients.

scRNA-Seq of tissue infiltrating $CD4^+CXCR5^+$ Tfh-like cells in IgG_4-RD

Although visualization by multicolor staining permits anatomic localization of Tfh cells in tissue, it provides only limited information. To better understand other cytokine-expressing Tfh cells in affected lesions with TLOs, we performed scRNA-Seq analysis (10× Genomics) of infiltrating Tfh cells from 4 IgG_4-RD patients (see Table E5 in this article's Online Repository at www.jacionline.org). The schematic strategy to study tissue infiltrating cells in IgG_4-RD is presented in Fig 3, *A*. We visualized selected marker genes in these gated Tfh cells. As shown in Fig 3, *B,* infiltrating $CD4^+CXCR5^+$ Tfh cells from IgG_4-RD tissues expressed *MAF, CD40LG, CTLA4, PDCD1,* and *ICOS;* these cells also expressed *IL10, IL21,* and *CXCL13.*

We compared expression values in the $CD4^+CXCR5^+$ Tfh cell cluster to selected cluster marker genes. The expression values of selected genes in each $CD4^+CXCR5^+$ Tfh cell, based on t-SNE analyses, are shown in Fig 3, *C*. The $CD4^+CXCR5^+$ Tfh cell phenotype was clustered into 6 distinct subtypes. Cells in cluster 0 were characterized by high expression levels of *CXCL13, PDCD1, IL21, BCL6,* and *ICOS,* suggesting they were "true" GC Tfh cells (Fig 3, *D*). Cells in cluster 1 were characterized by high expression levels of *IL10, LAG3, CTLA4,* and *PRDM1*. Cells in cluster 2 were characterized by high expression levels of *FOXP3* and *CTLA4,* suggesting they were regulatory follicular helper T (Tfr) phenotype cells.[22,23] Cells in cluster 4 and cluster 5 were characterized by high expression levels of *GZMA, GZMB,*

D, Multicolor immunofluorescence staining for T_H2, $GATA3^+$ Tfh, $GATA3^-$ Tfh, $CD4^+$ CTLs, and $CD4^+$ Other cells were done. Images of tissue specimens were acquired using the TissueGnostics TissueFAXS platform (see the Methods section in the Online Repository). *Left,* Absolute numbers per square millimeter and relative proportions of $CD4^+GATA3^+CXCR5^-$ T_H2 cells (*blue*), $CD4^+CXCR5^+GATA3^+$ Tfh cells (*red*), $CD4^+CXCR5^+GATA3^-$ Tfh cells (*green*), $CD4^+GZMA^+$ CTLs (*magenta*), and $CD4^+$ Other cells (*orange*) in affected tissues from 8 patients with KD and 20 patients with IgG_4-RD. *Right,* Relative proportions of T_H2 cells, $GATA3^+$ Tfh cells, $GATA3^-$ Tfh cells, $CD4^+$ CTLs, and $CD4^+$ Other cells between patients with KD (n = 8) and patients with IgG_4-RD (n = 20). Multiple comparisons are controlled for by Kruskal-Wallis test. Data are presented as means ± SEMs.

GZMK, GZMH, GZMM, PRF1, CRTAM, and *SLAMF7,* suggesting that were cytotoxic phenotype cells.

IL-10–expressing Tfh cells are prominent in IgG$_4$-RD patients

We presumed that the *IL-10*–expressing *LAG3*$^+$ Tfh cells would be a subset distinct from the Tfr cells.[22,23] We used scRNA-Seq to compare the transcriptomes between *IL-10*$^+$*CD4*$^+$ T cells and *IL-10*$^-$*CD4*$^+$ T cells in an affected lesion from a patient with IgG$_4$-RD (Fig 4, *A*). *IL-10*$^+$*CD4*$^+$ T cells expressed significantly higher levels of *LAG3* and *IL21* than did *IL-10*$^-$*CD4*$^+$ T cells. Although they did not express *FOXP3* and *EGR2,* IL-10$^+$CD4$^+$ T cells coexpressed *ICOS, LAG3, PRDM1, MAF,* and *CXCR5;* these were presumably Tfh-like phenotype cells that mainly produced *IL-10* (Fig 4, *B*). We thus suspected that most *IL-10*–secreting CD4$^+$ cells near germinal centers in tissues from IgG$_4$-RD patients were Tfh-like cells. We also noted that despite the absence of *FOXP3* expression, the *IL-10*$^+$ Tfh cells expressed *CTLA4* and exhibited low *IL-2* expression, which typically suppresses conventional Treg cell function. CTLA4 is a key transcriptional target of FOXP3 in Treg cells; robust CTLA4 expression combined with low IL-2 production is a good marker of Treg cell function, despite the absence of FOXP3 expression.[24] These results suggested that IL-10$^+$ Tfh cells in IgG$_4$-RD patients exhibit characteristics of Treg cells but are cells of the Tfh lineage.

We thus applied multicolor imaging for the IL-10–expressing CD4$^+$CXCR5$^+$ Tfh cells in affected lesions from IgG$_4$-RD patients and KD patients. Approximately 17% of CD4$^+$CXCR5$^+$ Tfh cells in IgG$_4$-RD patients expressed IL-10, while less than 7% of CD4$^+$CXCR5$^+$ Tfh cells expressed IL-10 in KD patients (Fig 4, *C*). We next examined whether infiltrating Tfh cells expressed IL-10 in normal tonsils and lymph nodes from IgG$_4$-RD patients. Approximately 20% of CD4$^+$CXCR5$^+$ Tfh cells expressed IL-10 in IgG$_4$-RD patients (Fig 4, *D*). The low frequency of IL-10 expression among Tfh cells was confirmed in normal tonsils. Taken together, these results suggested that the expanded IL-10–expressing Tfh cells in IgG$_4$-RD patients exhibit a gene expression profile that allows localization in and around germinal centers; they also support Treg cell function and abundant expression of *IL10.*

Cytotoxic Tfh cells are detected in IgG$_4$-RD patients

In our previous studies, we found clonally expanded CD4$^+$ CTLs in IgG$_4$-RD patients. Here, we found that cytotoxic phenotype Tfh cells in IgG$_4$-RD shared some genes (*SLAMF7, CRTAM, NKG7, GZMA, GZMK, CCL4,* and *CCL5*) with cytotoxic cells (Fig 3, *D,* and Fig 4, *E*). We also noted that that CD4$^+$CXCR5$^+$GXMK$^+$ Tfh cells were in cell-to-cell contact with CD19$^+$ B cells, as confirmed by nuclear distance measurements (Fig 4, *F*). Approximately 19% of CD4$^+$CXCR5$^+$ Tfh cells expressed GZMK in an IgG$_4$-RD patient.

Tfh13 cells are prominent in KD patients and sparse in IgG$_4$-RD patients

Tfh cells provide help to B cells during T-cell–dependent immune reactions, and they contribute to isotype switching, somatic hypermutation, memory B-cell generation, plasma cell differentiation, and germinal center formation.[1,2] To identify potentially pathogenic subsets of CD4$^+$ T cells that were clonally expanded in response to a potential antigen, we analyzed T-cell receptor β chain gene rearrangement using next-generation sequencing. We previously reported that IgG$_4$-RD patients exhibit large clonal expansions of CD4$^+$ CTLs that are the dominant T cells in diseased tissues.[13,21] As shown in Fig 2, *D,* Tfh and T$_H$2 cells were the dominant T-cell subsets in affected tissues from KD patients. We therefore initially analyzed the T-cell receptor β chain gene repertoire of circulating CD4$^+$CXCR5$^+$ Tfh (cTfh) cells and circulating CD4$^+$CXCR5$^-$CCR6$^-$CXCR3$^-$ T$_H$2 cells from the blood of a KD patient (Fig 5, *A*). We found that these circulating Tfh and T$_H$2 cells from the KD patients were more oligoclonally expanded compared to circulating naive CD4$^+$ T cells. cTfh cells from 2 IgG$_4$-RD patients were also oligoclonally expanded, while the repertoire of naive CD4$^+$ T cells from 2 healthy controls was highly diverse—that is, no dominant clones were observed in either individual (Fig 5, *B*). We next performed bulk RNA-Seq analysis of sorted activated PD-1$^+$CD4$^+$CXCR5$^+$ Tfh cells from a KD patient and an IgG$_4$-RD patient (Fig 5, *C*). The circulating PD-1$^+$ Tfh cells from the KD patient expressed higher levels of *IL4, IL5, IL13, STAT6,* and *GATA3* (all associated with type 2 immunity) compared to those in the IgG$_4$-RD patient.

We next performed *in situ* analyses of TLOs in affected lesions from KD and IgG$_4$-RD patients to identify activated Tfh phenotype cells. Notably, activated PD-1$^+$ICOS$^+$CXCR5$^+$ Tfh cells were detected near TLO-like structures containing germinal centers (Fig 5, *D*). GATA3-expressing ICOS$^+$ T cells, presumably Tfh phenotype cells, were also detected near TLO-like structures containing germinal centers. These GATA3$^+$ICOS$^+$ T cells comprised approximately 40% of ICOS$^+$ T cells in affected tissue lesions from KD patients, while they comprised less than 10% of ICOS$^+$ T cells from IgG$_4$-RD patients (Fig 5, *E*). Finally, we examined TLOs in affected lesions from KD patients to quantify Tfh cells that expressed IL-13 *in situ.* IL-13$^+$ICOS$^+$GATA3$^+$ T cells were abundant in KD patients. In a lesion from a patient with KD, approximately 54% and 12% of ICOS$^+$GATA3$^+$ T cells expressed IL-13 and IL-5, respectively (Fig 5, *F*). IL-13–expressing CD4$^+$CXCR5$^+$ Tfh cells were also abundant in KD tissue lesions, although they were rare in IgG$_4$-RD tissue lesions (Fig 5, *G*). Most IL-13–expressing Tfh cells were located near TLO-like structures in tissues from KD patients. Higher serum IgE concentrations were present in KD patients who had greater proportions of IL-13$^+$ Tfh cells in these tissues (Fig 5, *H*). We speculate that the expansion of these IL-13–expressing Tfh cells, presumably the IL-13–expressing GATA3$^+$ Tfh13 cells associated with high-affinity IgE,[14] might represent an important disease-related Tfh subset in KD patients.

IgG$_1$- and *IgG$_4$*-expressing B cells in IgG$_4$-RD tissues were oligoclonally expanded

To identify potentially pathogenic subsets of infiltrating B cells that were clonally expanded in response to a potential antigen, we analyzed B-cell receptor chain gene rearrangements using single-cell repertoire analysis (10× Genomics). The schematic strategy for the B-cell receptor repertoire to study tissue-infiltrating cells from salivary glands from 3 IgG$_4$-RD patients is shown in Fig 6, *A*. We analyzed the frequencies of immunoglobulin isotypes using B-cell receptor repertoire analysis in affected lesions from a patient with IgG$_4$-RD. Large clonal expansions of *IgG$_1$*- and *IgG$_4$*-expressing B cells were particularly prominent (Fig E3, *A*). In affected IgG$_4$-RD lesions with TLOs, both *IGHG1* and *IGHG4*

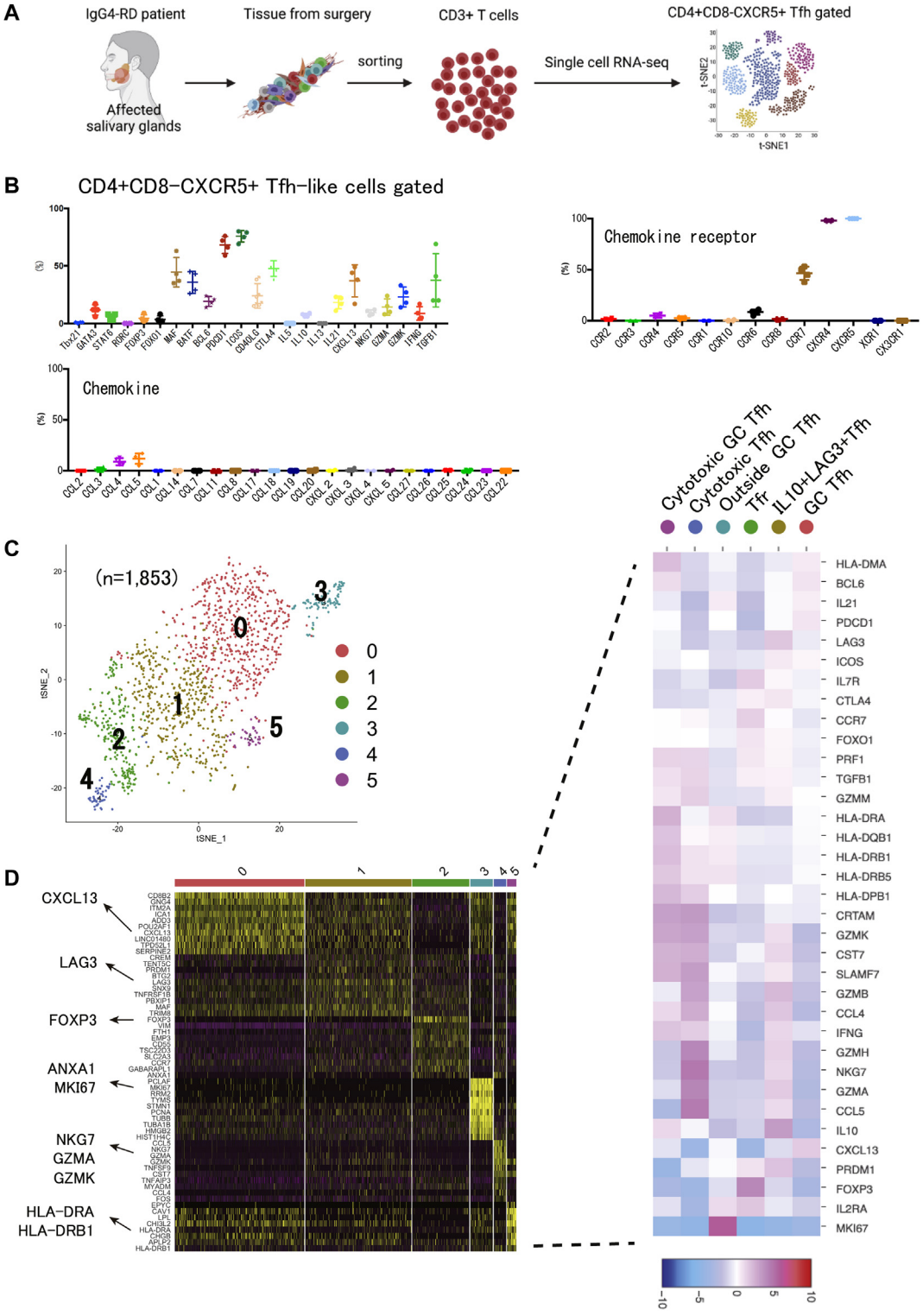

FIG 3. Transcriptomic profiling of infiltrating *CD4*$^+$*CXCR5*$^+$ Tfh cells in affected salivary glands (SGs) from IgG_4-RD. **A,** Sorted CD3$^+$CD19$^-$ T cells from affected SGs from patients with IgG_4-RD were gated into *CD4*$^+$*CD8A*$^-$*CXCR5*$^+$ Tfh-like cells (n = 4). **B,** scRNA-Seq profiling revealed the expression patterns of Tfh-related cytokine-, chemokine-, chemokine receptor–, membrane-, and transcription factor–related genes in *CD4*$^+$*CXCR5*$^+$ Tfh cells in affected SGs from patients with IgG_4-RD (n = 4). **C,** Six clusters across 1853 C*D4*$^+$ *CXCR5*$^+$ Tfh cells, identified via t-SNE visualization. Schematic representation of single-cell transcriptome experiments from submandibular gland sample collection to clustering of *CD4*$^+$*CXCR5*$^+$ Tfh-like cells in a patient with IgG_4-RD (patient 4). **D,** *Left,* Heat map shows top 10 gene expression patterns in *CD4*$^+$*CXCR5*$^+$ Tfh cells among the 6 clusters in a patient with IgG_4-RD (patient 4). *Right,* Selected gene expression patterns in *CD4*$^+$*CXCR5*$^+$ Tfh cells in the 6 clusters in a patient with IgG_4-RD (patient 4).

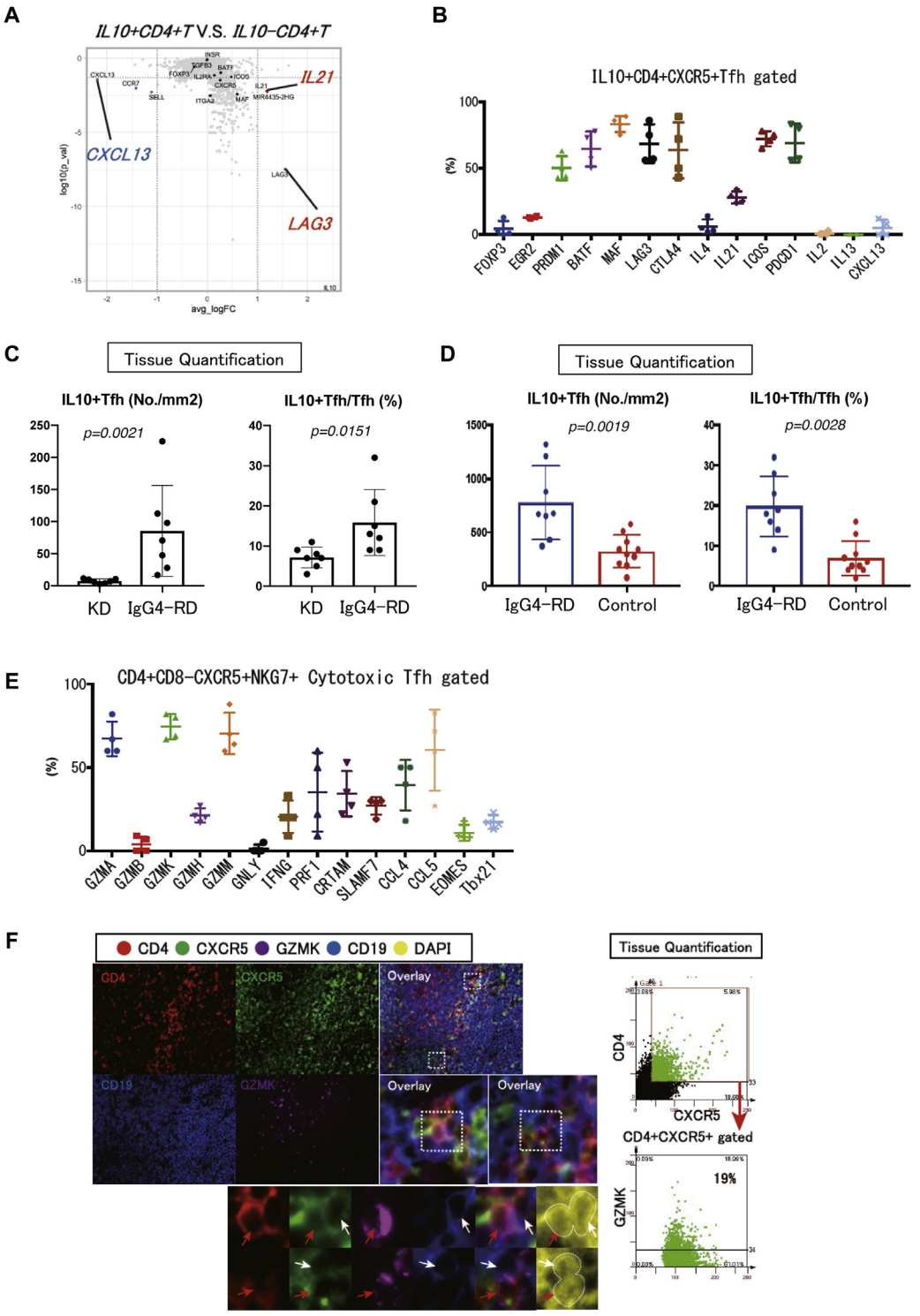

FIG 4. Transcriptomic profiling of *IL-10*–expressing *LAG3*$^+$ Tfh cells and cytotoxic Tfh cells in affected salivary glands (SGs) from IgG_4-RD. **A,** Volcano plot showing single-cell RNA-Seq analysis of gene expression in *IL-10*–expressing and nonexpressing *CD4*$^+$ T cells in affected tissue from a patient with IgG_4-RD. Differential expression patterns of 28,000 genes were investigated by scRNA-Seq. Violin plot showing *LAG3* gene expression in *IL-10*–expressing and nonexpressing *CD4*$^+$ T cells in affected tissue from a patient with IgG_4-RD. **B,** scRNA-Seq profiling revealed the expression patterns of Tfh-related cytokine-, chemokine-, membrane-, and transcription factor–related genes in *IL-10*$^+$ *CD4*$^+$ *CXCR5*$^+$ Tfh cells in affected tissues from patients with IgG_4-RD (n = 4). **C,** *Left,* Absolute numbers of IL-10$^+$CD4$^+$CXCR5$^+$ Tfh cells in affected tissues from patients with KD (n = 7) and patients with IgG_4-RD (n = 7). *Right,* Relative proportions of CD4$^+$CXCR5$^+$ Tfh cells expressing IL-10 in affected tissues from patients with KD (n = 7) and patients with IgG_4-RD (n = 7). *P* value was determined by Student *t* test. **D,** *Left,* Absolute numbers of IL-10$^+$CD4$^+$CXCR5$^+$ Tfh cells in

were abundant among class-switched isotypes, but *IGHE* was sparse (Fig 6, *B*). We hypothesized that antigen-driven B cells would demonstrate some degree of B-cell receptor sharing and that this may be reflected in oligoclonality. However, we found no evidence for this. The V-J gene segment usage of expanded clones was not identical across 3 IgG_4-RD subjects, and there were no clones with shared CDR3 sequences across individuals (see Fig E3, *B,* in the Online Repository at www.jacionline.org).

Frequency of *AICDA*$^+$ B cells expressing receptors for *IL-4, IL-10,* and *IL-21* correlates with IgG_4 expression

We compared expression values in the B-cell cluster to selected cluster marker genes. For these selected genes, expression values in each B cell, based on t-SNE analysis, are shown in Fig 7, *A*. The B-cell phenotype was clustered into 7 distinct subtypes (see Fig E4). We next focused on an IgG_4-associated subpopulation in the B-cell cluster. As shown in Fig 7, *B,* cells in cluster 2 were characterized by high expression levels of *CD27, CD38, CXCR5, BCL6, MME, CD40, AICDA, IGHG4, IL4R, IL10RA,* and *IL21RA*. These findings suggested that the cluster 2 population comprised activated B cells undergoing class switching. Furthermore, cells in cluster 2 exhibited low expression levels of *IGHD* and *IGHM*. In contrast, cells in cluster 4 highly expressed *IGHG4, CD38, CD27,* and *CD138;* thus, cluster 4 population presumably comprised plasma cells. We next analyzed infiltrating *AICDA*$^+$*CD19*$^+$ B cells in affected lesions from 3 IgG_4-RD patients using scRNA-Seq. Most infiltrating *AICDA*$^+$*CD19*$^+$ B cells expressed *IL4R, IL10RA,* and *IL21R,* but not *IL13R* (Fig 7, *C*). Most *AICDA*$^+$*CD19*$^+$*IL-4R*$^+$*IL-10RA*$^+$*IL-21R*$^+$ B cells expressed a comparatively high level of *IGHG4* (Fig 7, *D*).

Allergic fibrosis in KD is linked to activated type 2 immune cells

Eosinophilic microabscesses and eosinophil-infiltrated neural fibers are typical features in KD patients. Eosinophils were expanded in affected tissues from KD patients compared to affected tissues from IgG_4-RD patients (see Fig E5, *A,* in the Online Repository at www.jacionline.org). Galectin-10 is released by activated eosinophils during type 2 immune reactions.[25,26] Galectin-10–positive cells (ie, activated eosinophils) were expanded in affected lesions from KD patients compared to IgG_4-RD patients (Fig E5, *B*). Osteopontin (OPN) is a glycoprotein that exhibits fibrogenic and angiogenic properties; it has also been implicated in allergic disease. Thus, we explored the major cellular source of OPN in affected lesions from patients with KD and patients with IgG_4-RD. OPN$^+$Siglec-8$^+$ eosinophils were sparse in patients with IgG_4-RD (Fig E5, *C*), but in contrast were abundant in patients with KD (Fig E5, *C*); most OPN-stained cells also expressed Siglec-8 in patients with KD. Furthermore, approximately 60% of Siglec-8$^+$ eosinophils expressed OPN in a patient with KD, while less than 20% of Siglec-8$^+$ eosinophils expressed OPN in a patient with IgG_4-RD (Fig E5, *C*). Finally, amphiregulin-positive CD4$^+$ T cells were detected and abundant in affected tissue from patients with KD (Fig E5, *D*).

Type 2 cytokines are produced by activated IgE-coated c-kit$^+$ mast cells in KD patients

A previous report[27] showed that IL-4–producing cells were abundant in affected tissues from KD patients. To our knowledge, no previous study has used a quantitative approach to describe IL-4–expressing cells in affected lesions from KD patients. Notably, IL-4 is expressed by T_H2 and Tfh cells. Mast cells also play central roles in IgE-mediated allergic diseases by releasing IL-4, IL-5, and IL-13. We thus speculated that a subset of IL-4–producing cells might be mast cells in KD patients. We used immunofluorescence to compare the numbers of mast cells (detected by c-kit staining) among KD patients and IgG_4-RD. We found that IgE$^+$c-kit$^+$ activated mast cells expressed IL-4 in affected tissues from a patient with KD (Fig E5, *E*). Furthermore, IL-4$^+$c-kit$^+$IgE$^+$ mast cells were abundant in KD patients. Some IgG_4-RD patients exhibited infiltrating IL-4$^+$c-kit$^+$IgE$^+$ mast cells in their affected lesions. We subsequently analyzed IL-5 and IL-13 production by activated mast cells. Importantly, IL-5–expressing c-kit$^+$IgE$^+$ mast cells and IL-13–expressing mast cells were abundant in KD patients but sparse in IgG_4-RD patients.

Inflammatory-related cytokines and type 2 immunity–related cytokines in IgG_4-RD

We applied scRNA-Seq to profile tissue infiltrating all cells in fresh affected salivary glands from IgG_4-RD patients. Some nonallergic IgG_4-RD patients exhibit elevated serum IgE.[9] We thus obtained affected salivary glands from 3 nonallergic IgG_4-RD patients with high serum IgE. We visualized selected marker genes for inflammatory- and type 2 immunity–related cytokines using t-SNE Map (see Fig E6, *A,* in the Online Repository at www.jacionline.org). Most inflammatory-related genes (*GZMA, GZMK, IFNG, PRF1, TNF,* and *TGFB1*) are expressed in T cells from IgG_4-RD tissue (Fig 4, *D*). Gene expression of IL-6, a proinflammatory cytokine, was sparse in IgG_4-RD tissue (Fig E6, *A*). In contrast, type 2 immunity–related genes (*IL5, IL13, IL25, IL33, TSLP, IGHE,* and *IL1RL1*) were sparse in IgG_4-RD tissue (Fig E6, *B*). Some CD14$^+$ monocytes express *TSLP* and *IL33,* but at low levels.

DISCUSSION

In T-cell–dependent immune responses, Tfh cells are the primary helper T cells responsible for directing the affinity, longevity, and isotype of antibodies produced by B cells. Specific

draining lymph nodes from 8 patients with IgG_4-RD and tonsils from 10 healthy controls. *Right,* Relative proportions of CD4$^+$CXCR5$^+$ Tfh cells expressing IL-10 in draining lymph nodes from 8 patients with IgG_4-RD and tonsils from 10 healthy controls. *P* value was determined by Student *t* test. **E,** Single-cell RNA-seq profiling revealed the expression patterns of Tfh-related cytokine-, chemokine-, membrane-, and transcription factor–related genes in *CD4*$^+$*CD8*$^-$*CXCR5*$^+$*NKG7*$^+$ cytotoxic Tfh cells in affected tissues from patients with IgG_4-RD (n = 4). **F,** *Left,* Multicolor immunofluorescence staining of CD4 (red), CXCR5 (green), GZMK (magenta), CD19 (blue), and DAPI (yellow) in affected tissue from a patient with IgG_4-RD. *Right,* Quantification of CD4$^+$CXCR5$^+$GZMK$^+$ cells in affected tissue from a patient with IgG_4-RD.

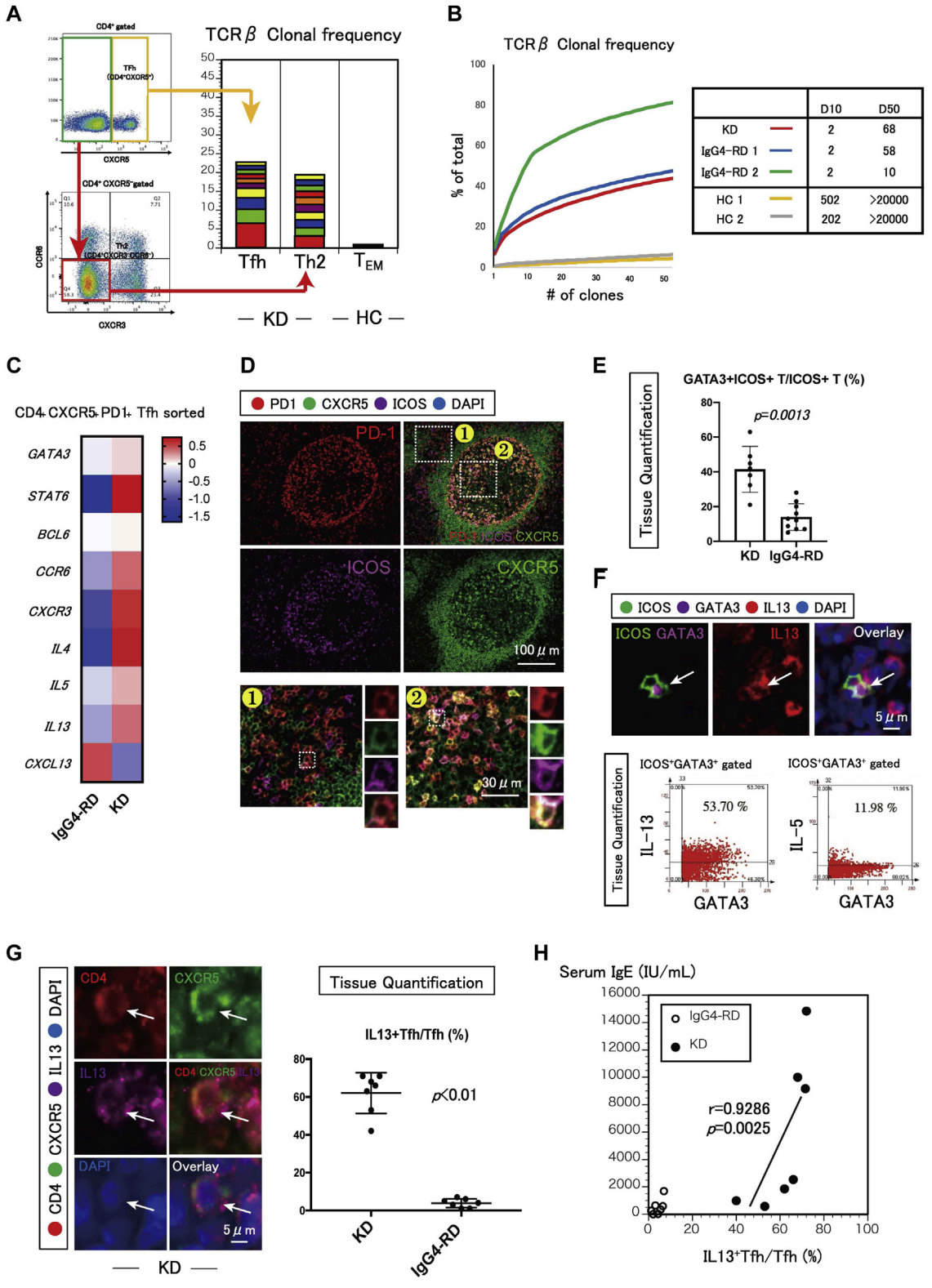

FIG 5. IL-13–expressing Tfh cells are abundant in patients with KD. **A,** Stacked bar chart indicating frequencies of top 10 TCR β clones in circulating $CD4^+CXCR5^+$ Tfh cells and circulating $CD4^+CXCR5^-CXCR3^-CCR6^-$ T_H2 cells from a patient with KD and circulating $CD4^+CD27^-CD62L^-$ effector memory T (T_{EM}) cells from a healthy control. **B,** Distributions of clone frequencies in circulating $CD4^+CXCR5^+$ Tfh cells from 2 patients with IgG_4-RD (*blue* and *green*) and a patient with KD (*red*) compared to T_{EM} cell frequencies from 2 healthy controls (*yellow* and *gray*). Minimum numbers of clones comprising 10% (D10) and 50% (D50) of clone diversity are shown. **C,** Heat map depicting differentially expressed T_H2- and Tfh-related genes in circulating $CD4^+CXCR5^+PD\text{-}1^+$ Tfh cells from patients with KD and IgG_4-RD (n = 1 each). **D,** Multicolor immunofluorescence staining of PD-1 (*red*), CXCR5

cytokine-producing Tfh cells contribute to distinct isotype switching events.[1,2] Indeed, distinct $CD4^+CXCR5^+$ Tfh cells are abundant in affected lesions from KD patients and IgG_4-RD patients, which are diseases in which there is prominent switching of activated B cells to 2 different immunoglobulin isotypes. Here we described abundant infiltration of distinct Tfh cells in these 2 disorders. Our novel findings were as follows: (1) infiltrating IL-13–expressing Tfh cells were abundant in affected lesions of patients with allergic disorders (eg, KD patients); (2) infiltrating IL-13–expressing Tfh cells were sparse in IgG_4-RD; (3) infiltrating IL-10–expressing Tfh cells, but not Treg cells or Tfr cells, were abundant in IgG_4-RD patients and expressed *IL-21* and *LAG3*; (4) the frequency of $AICDA^+CD19^+$ B cells expressing receptors for *IL4, IL10,* and *IL21* correlated with IgG_4 expression in IgG_4-RD; and (5) distinct infiltrating cell types characterize 2 distinct types of fibrotic disorders: allergic fibrosis (driven by type 2 immune cells) and inflammatory fibrosis (driven by cytotoxic T cells).

Class switching to IgG_4 is poorly understood. $CD4^+$ T cells can stimulate IgM-positive B cells to switch to IgG_4 and IgE in the presence of added IL-4.[28] *In vitro* findings have suggested that IL-10 indirectly contributes to IgG_4 class switching by facilitating IL-4–mediated switching to IgG_4 rather than IgE.[10] Previous work distinguished Tfh cells by identifying a distinctive *IL4* enhancer locus bound by BATF in Tfh cells that is distinct from the T_H2 DNA regulatory element for IL-4, IL-5, and IL-13 bound by GATA3.[29] Subsequent research indicated that IL-4–positive Tfh cells instruct plasma cells to switch from IgM to IgE via BATF-driven IL-4, thus producing low-affinity IgE antibodies.[14] To our knowledge, Tfh cells expressing other cytokines have not been assessed in IgG_4-RD patients at the single-cell level. In this study, we found that IL-10– and IL-21–expressing Tfh cells were abundant in IgG_4-RD patients compared to levels in patients with allergic disorders. Using scRNA-Seq analysis of infiltrating lymphocytes, we confirmed that the expanded IL-10–expressing $CD4^+CXCR5^+$ Tfh cells in affected lesions from IgG_4-RD patients coexpressed *IL21, PDCD1,* and *ICOS,* but not *Foxp3;* these cells presumably differed from Treg or Tfr phenotype cells. A study of IL-10 and IL-21 double-reporter mice revealed that $IL\text{-}10^+IL\text{-}21^+CXCR5^+PD\text{-}1^+$ Tfh cells were distinct from Foxp3-expressing Tfr cells.[30] In contrast, the $CD4^+CXCR5^+Foxp3^+$ Tfr cells population in lymph nodes from IgG_4-RD patients was also abundant compared to that in healthy tonsils (data not shown). Thus, these Tfr cells in IgG_4-RD patients require further exploration. Notably, we limited our tissue analysis to IgG_4 class-switched B cells, but our results suggest that the amounts of IL-4, IL-10, and IL-21 produced by disease-specific Tfh cells may contribute to specific IgG_4 class switching in IgG_4-RD patients (Fig 8).

We also found abundant cytotoxic Tfh cells and Tfr cells in IgG_4-RD patients. However, additional research for these cytotoxic Tfh cells and Tfr cells is required to further elucidate the pathogenesis of IgG_4-RD.

The exact source of the elevated IgG_4 and IgE in the blood and/or tissue in IgG_4-RD patients is unknown. Tissue IgE-positive memory B cells and plasma cells may emerge directly from germinal centers or through indirect class switching from other intermediate antibody isotype such as IgG_1 to IgG_4.[31,32] The majority of IgE-positive cells derive from somatically hypermutated IgG_1-expressing cells, as demonstrated from analysis of immunoglobulin-heavy regions in blood of allergy patients, and indirect isotype switching from IgG_4 to IgE contributes to the IgE pool.[33] In this study, we demonstrated that a rare IL-13–expressing Tfh cell population, which coexpressed GATA3 and Bcl6, was dominant in affected tissues from KD patients; however, this population was sparse in IgG_4-RD patients despite the presence of high serum IgE levels. Human Tfh cells expressing GATA3, IL-13, and IL-4 have been previously identified.[14] Furthermore, Tfh13 cells in mice and humans have an unusual cytokine profile ($IL\text{-}4^{hi}IL\text{-}13^{hi}$) and coexpress the BCL6 and GATA3 transcription factors.[14] These Tfh13 cells are required for production of high-affinity (but not low-affinity) IgE and subsequent allergen-induced anaphylaxis.[14] We speculated that the expansion of these IL-13–expressing Tfh cells might represent an important disease-related Tfh subset, which contributes to specific class-switching and affinity-maturation events in KD patients (Fig 8).

Fibrosis is the end result of chronic inflammatory reactions such as allergic responses, infections, autoimmune reactions, tissue injury, and radiation. Fibrotic diseases likely have many different etiologies, and they may not all be driven by $CD4^+$ T cells. Our recent findings implicated $CD4^+$ CTLs in the induction of apoptotic cell death and subsequently fibrosis in IgG_4-RD,[13,15] systemic sclerosis,[34] Covid-19,[3] and fibrosing mediastinitis, a disease linked to *Histoplasma capsulatum* infection.[35]

In contrast, type 2 immune cells and their cytokines (IL-4, IL-5, IL-9, and IL-13) represent a central population in the pathogenesis of allergic inflammation and fibrosis.[16] Complex inflammatory reactions involve eosinophils, basophils, mast cells, ILC2s, T_H2 cells, and subclasses of IgE antibodies; these components play important roles in the pathogenesis of many allergic and fibrotic disorders. IL-5 is a key cytokine involved in eosinophil development and activation. Lesional inflammation causes recruitment of eosinophils with inflammatory features.[16] Morimoto et al[36] reported that interactions between pathogenic memory T_H2 cells and OPN-producing eosinophils may be a potential target for the treatment of fibrosis induced by chronic allergic

(*green*), ICOS (*magenta*), and DAPI (*blue*) in tissue inside and outside a germinal center in a patient with KD. **E,** Relative proportions of $ICOS^+$ T cells expressing GATA3 in tissue from patients with KD (n = 7) and IgG_4-RD (n = 10). *P* value was determined by Student *t* test. **F,** Multicolor immunofluorescence staining of ICOS (*green*), GATA3 (*magenta*), IL-13 (*red*), and DAPI (*blue*) in affected tissue from a patient with KD. Scatterplots depict mean fluorescence intensity per cell for each immunostained molecule in tissue from a patient with KD. Quantification of $ICOS^+GATA3^+IL\text{-}13^+$ T cells and $ICOS^+GATA3^+IL\text{-}5^+$ T cells in tissue from a patient with KD. **G,** Multicolor immunofluorescence staining of CD4 (*red*), CXCR5 (*green*), IL-13 (*magenta*), and DAPI (*blue*) in tissue from a patient with KD. Relative proportions of $CD4^+CXCR5^+$ Tfh cells expressing IL-13 in tissue from patients with KD (n = 7) and IgG_4-RD (n = 7). *P* value was determined by Student *t* test. **H,** Higher percentage of $IL\text{-}13^+$ Tfh cells in tissues from patients with KD (n = 7) correlated with higher serum IgE concentrations compared to IgG_4-RD (n = 7). Correlation coefficients and *P* values were determined by Spearman rank correlations.

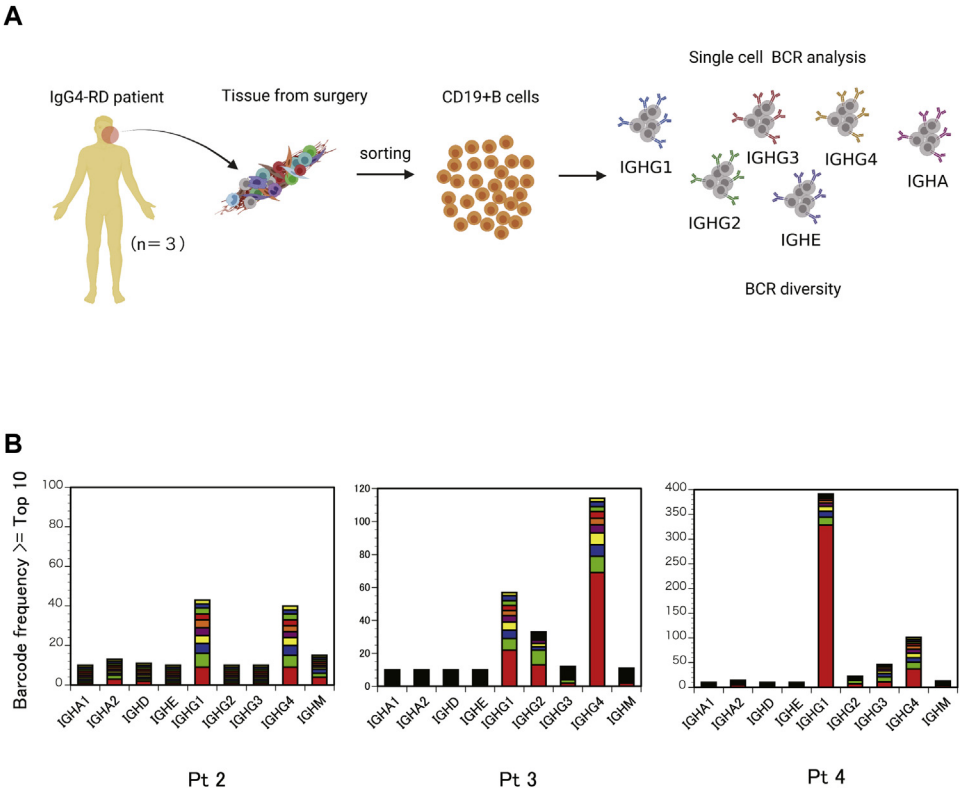

FIG 6. Single-cell B-cell receptor analysis of affected lesions from patients with IgG_4-RD. **A,** Sorted CD3−CD19$^+$ B cells from affected salivary glands (SGs) with IgG_4-RD were examined for B-cell receptor repertoire analyses. **B,** Stacked bar chart indicating barcode frequencies of top 10 B-cell receptor clones of immunoglobulin heavy chain in B cells, from 3 patients with IgG_4-RD according to scRNA-Seq and B-cell receptor profiling, using 10× Genomics Loupe V(D)J Browser.

disorders. Some reports suggested that IgG_4-RD appears to involve some of the same pathogenic mechanisms observed in allergic disease, such as T_H2 and Treg activation, IgG_4 and IgE hypersecretion and blood/tissue eosinophilia.[37] Multiple cell types associated with a type 2 immune response are found at sites of affected lesions in KD patients compared to IgG_4-RD. Amphiregulin has been shown to reprogram the transcriptome of eosinophils toward an inflammatory state that induces secretion of OPN, an extracellular matrix protein associated with fibrotic disorders.[36] Charcot-Leyden crystal protein (also known as galectin-10) is required for eosinophile granulogenesis.[26] Galectin-10 is a hallmark of eosinophil death and can persist in tissues for months. Recent genome-wide genetic and epigenetic association studies found a strong association of total IgE levels with hypomethylation at the *LGALS10* gene locus, suggesting that the eosinophil galectin-10 axis may also be a trigger for IgE synthesis in human type 2 immune disease.[25,38] In a recent report, increased blood ILC2 were linked to blood eosinophilia, elevated IgE, and itching in KD.[39] In our staining data, we also noticed that a large number of CD4-negative, GATA3-positive cells infiltrated KD tissues (Fig E2, *A*), suggesting that these cells may be ILC2s or related cells. These GATA3-positive non–T cells in lesions will be more thoroughly investigated in future studies. We found that type 2 immune cells were sparse in IgG_4-RD patients compared to that in KD. Cross-linking of high-affinity IgE on the surface of mast cells leads to the release of chemical mediators that precipitate anaphylaxis.[40] Studies from patients with food allergies and murine models of allergic disease indicate that high-affinity (but not low-affinity) IgE induces mast cell degranulation and anaphylaxis.[40] Mast cells capture monomeric IgE on their surface using the high-affinity FcεRI, and antigen-mediated cross-linking of FcεRI-bound IgE leads to mast cell activation and the release of allergic mediators. High-affinity (but not low-affinity) IgE might be detected in germinal centers from KD patients. Activated mast cells produce profibrotic factors including TGF-β1, IL-4, IL-13, tryptase, chymase, and chemokines that promote fibroblast activation in human fibrotic disease.[41] Most IL-13 is produced by T_H2, Tfh13, and activated mast cells in affected lesions from KD patients. IL-13 can also directly promote fibrosis by stimulating proliferation or collagen production by fibroblasts, as well as fibroblast differentiation into myofibroblasts.[42] In KD patients, activated eosinophils and mast cells contribute to a chronic inflammatory response.[11] Our findings suggest 2 types of fibrosis, allergic fibrosis (driven by type 2 cells) and inflammatory fibrosis (driven by cytotoxic T cells), in KD and IgG_4-RD.

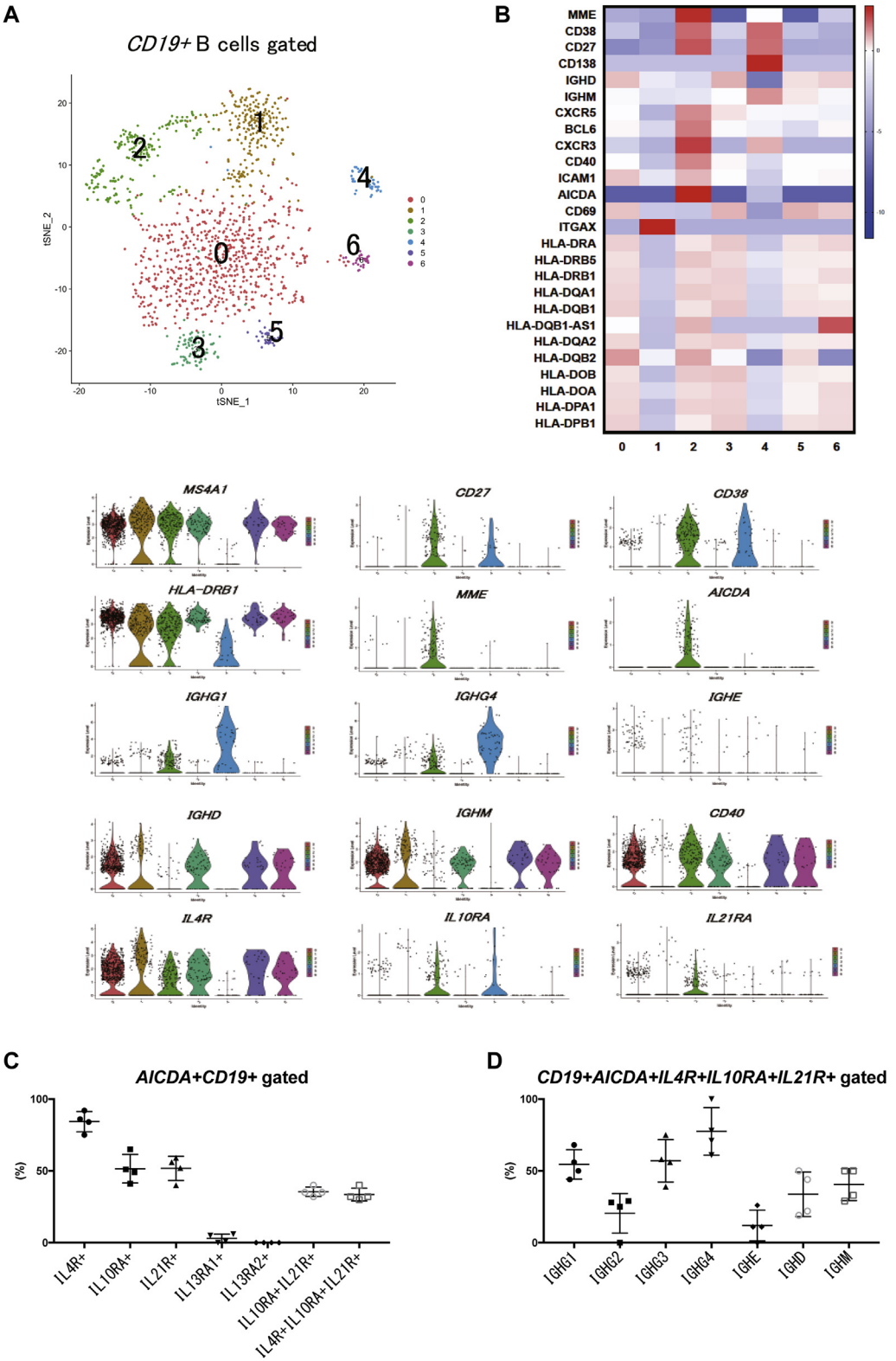

FIG 7. Single-cell B-cell transcriptome analysis of affected lesions from patients with IgG_4-RD. **A,** Seven clusters across 1245 $CD19^+$ cells identified via t-SNE visualization. Schematic representation of single-cell transcriptome experiments from submandibular gland sample collection revealed clustering of $CD19^+$ B cells in a patient with IgG_4-RD (patient 3). **B,** *Top,* Selected gene expression patterns in $CD19^+$ B cells among the 7 clusters in a patient with IgG_4-RD (patient 3). *Bottom,* Violin plot showing gene expression patterns according to t-SNE clusters (patient 3). **C,** scRNA-Seq profiling revealed the expression patterns of interleukin receptor genes in $AICDA^+CD19^+$ B cells in affected tissues from patients with IgG_4-RD (n = 4). **D,** scRNA-Seq profiling revealed the percentages of *IGHG1, IGHG2, IGHG3, IGHG4, IGHE, IGHD,* and *IGHM* in $AICDA^+CD19^+IL\text{-}4R^+IL\text{-}10RA^+IL\text{-}21R^+$ B cells in affected tissues from patients with IgG_4-RD (n = 4).

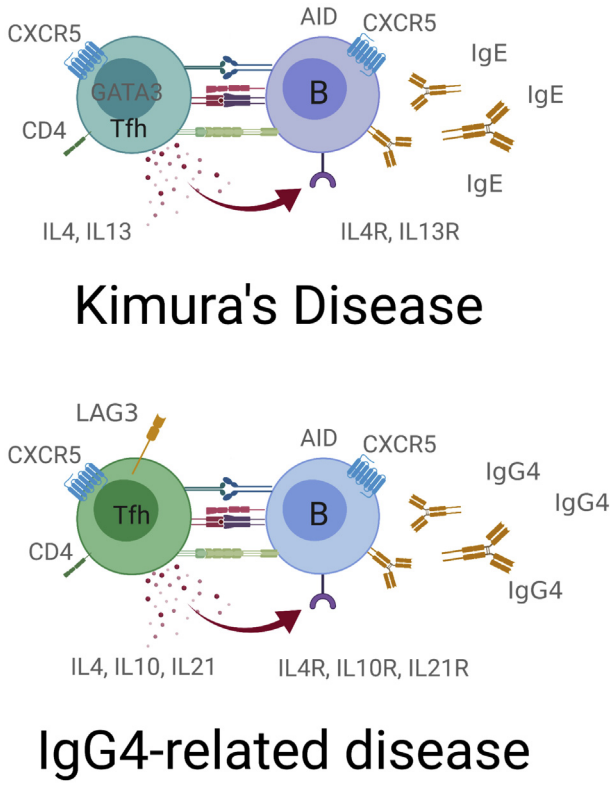

FIG 8. Model of IgG_4 class switching by IL-10^+ Tfh cells in IgG_4-related disease, which contrasts with IgE class switching by IL-13^+ Tfh cells observed in KD. Schematic overview of the proposed disease class switching mechanisms in patients with KD and patients with IgG_4-RD. Expansion of infiltrating IL-10^+ Tfh cells, but not Tfh13 cells, might contribute to IgG_4 isotype switching in SLOs and TLOs of patients with IgG_4-RD. In contrast, expansion of infiltrating Tfh13 cells might contribute to high-affinity IgE secretion by B cells in KD.

We thank Ryan Chastain-Gross, PhD, and Gabrielle White Wolf, PhD, from Edanz (https://jp.edanz.com/ac), for editorial work.

Key messages

- **A novel IL-10–expressing Tfh-like cell subset, but not Treg cells or Tfr cells, was detected in affected tissues from patients with IgG_4-RD, and these IL-10–expressing Tfh-like cells expressed *LAG3* and *PRDM1*.**
- **The frequency of $AICDA^+CD19^+$ B cells expressing receptors for IL-10 and IL-21 correlated with IgG_4 expression in IgG_4-RD.**
- **An IL-13–expressing Tfh-like cell subset was detected in tissue lesions from patients with KD but not patients with IgG_4-RD.**

REFERENCES

1. Crotty S. Follicular helper CD4 T cells (TFH). Annu Rev Immunol 2011;29:621-63.
2. Crotty S. A brief history of T cell help to B cells. Nat Rev Immunol 2015;15:185-9.
3. Kaneko N, Kuo HH, Boucau J, Farmer JR, Allard-Chamard H, Mahajan VS, et al. Loss of Bcl-6–expressing T follicular helper cells and germinal centers in Covid-19. Cell 2020;183:143-57.e13.
4. Roco JA, Mesin L, Binder SC, Nefzger C, Gonzalez-Figueroa P, Canete PF, et al. Class-switch recombination occurs infrequently in germinal centers. Immunity 2019;51:337-50.e7.
5. Maehara T, Mattoo H, Mahajan VS, Murphy SJ, Yuen GJ, Ishiguro N, et al. The expansion in lymphoid organs of IL-4^+BATF$^+$ T follicular helper cells is linked to IgG_4 class switching *in vivo*. Life Sci Alliance 2018;1:e201800050.
6. Kamisawa T, Zen Y, Pillai S, Stone JH. IgG_4-related disease. Lancet 2015;385:1460-71.
7. Mattoo H, Mahajan VS, Della-Torre E, Sekigami Y, Carruthers M, Wallace ZS, et al. *De novo* oligoclonal expansions of circulating plasmablasts in active and relapsing IgG_4-related disease. J Allergy Clin Immunol 2014;134:679-87.
8. Maehara T, Moriyama M, Nakashima H, Miyake K, Hayashida JN, Tanaka A, et al. Interleukin-21 contributes to germinal centre formation and immunoglobulin G_4 production in IgG_4-related dacryoadenitis and sialoadenitis, so-called Mikulicz's disease. Ann Rheum Dis 2012;71:2011-9.
9. Della Torre E, Mattoo H, Mahajan VS, Carruthers M, Pillai S, Stone JH. Prevalence of atopy, eosinophilia, and IgE elevation in IgG_4-related disease. Allergy 2014;69:269-72.
10. Jeannin P, Lecoanet S, Delneste Y, Gauchat JF, Bonnefoy JY. IgE versus IgG_4 production can be differentially regulated by IL-10. J Immunol 1998;160:3555-61.
11. Chen H, Thompson LD, Aguilera NS, Abbondanzo SL. Kimura disease: a clinicopathologic study of 21 cases. Am J Surg Pathol 2004;28:505-13.
12. Mattoo H, Della-Torre E, Mahajan VS, Stone JH, Pillai S. Circulating Th2 memory cells in IgG_4-related disease are restricted to a defined subset of subjects with atopy. Allergy 2014;69:399-402.
13. Mattoo H, Mahajan VS, Maehara T, Deshpande V, Della-Torre E, Wallace ZS, et al. Clonal expansion of $CD4^+$ cytotoxic T lymphocytes in patients with IgG_4-related disease. J Allergy Clin Immunol 2016;138:825-38.
14. Gowthaman U, Chen JS, Zhang B, Flynn WF, Lu Y, Song W, et al. Identification of a T follicular helper cell subset that drives anaphylactic IgE. Science 2019;365:eaaw6433.
15. Perugino CA, Kaneko N, Maehara T, Mattoo H, Kers J, Allard-Chamard H, et al. $CD4^+$ and $CD8^+$ cytotoxic T lymphocytes may induce mesenchymal cell apoptosis in IgG_4-related disease. J Allergy Clin Immunol 2021;147:368-82.
16. Gieseck RL 3rd, Wilson MS, Wynn TA. Type 2 immunity in tissue repair and fibrosis. Nat Rev Immunol 2018;18:62-76.
17. Umehara H, Okazaki K, Masaki Y, Kawano M, Yamamoto M, Saeki T, et al. A novel clinical entity, IgG_4-related disease (IgG_4RD): general concept and details. Mod Rheumatol 2012;22:1-14.
18. Vitali C, Bombardieri S, Jonsson R, Moutsopoulos HM, Alexander EL, Carsons SE, et al. Classification criteria for Sjogren's syndrome: a revised version of the European criteria proposed by the American-European Consensus Group. Ann Rheum Dis 2002;61:554-8.
19. Ecker RC, Steiner GE. Microscopy-based multicolor tissue cytometry at the single-cell level. Cytometry A 2004;59:182-90.
20. Ruddle NH. Lymphatic vessels and tertiary lymphoid organs. J Clin Invest 2014;124:953-9.
21. Maehara T, Mattoo H, Ohta M, Mahajan VS, Moriyama M, Yamauchi M, et al. Lesional $CD4^+$ IFN-gamma$^+$ cytotoxic T lymphocytes in IgG_4-related dacryoadenitis and sialoadenitis. Ann Rheum Dis 2017;76:377-85.
22. Chung Y, Tanaka S, Chu F, Nurieva RI, Martinez GJ, Rawal S, et al. Follicular regulatory T cells expressing Foxp3 and Bcl-6 suppress germinal center reactions. Nat Med 2011;17:983-8.
23. Linterman MA, Pierson W, Lee SK, Kallies A, Kawamoto S, Rayner TF, et al. $Foxp3^+$ follicular regulatory T cells control the germinal center response. Nat Med 2011;17:975-82.
24. Yamaguchi T, Kishi A, Osaki M, Morikawa H, Prieto-Martin P, Wing K, et al. Construction of self-recognizing regulatory T cells from conventional T cells by controlling CTLA-4 and IL-2 expression. Proc Natl Acad Sci U S A 2013;110:E2116-25.
25. Persson EK, Verstraete K, Heyndrickx I, Gevaert E, Aegerter H, Percier JM, et al. Protein crystallization promotes type 2 immunity and is reversible by antibody treatment. Science 2019;364:eaaw4295.
26. Grozdanovic MM, Doyle CB, Liu L, Maybruck BT, Kwatia MA, Thiyagarajan N, et al. Charcot-Leyden crystal protein/galectin-10 interacts with cationic ribonucleases and is required for eosinophil granulogenesis. J Allergy Clin Immunol 2020;146:377-89.e10.
27. Kimura Y, Pawankar R, Aoki M, Niimi Y, Kawana S. Mast cells and T cells in Kimura's disease express increased levels of interleukin-4, interleukin-5, eotaxin and RANTES. Clin Exp Allergy 2002;32:1787-93.
28. Gascan H, Gauchat JF, Roncarolo MG, Yssel H, Spits H, de Vries JE. Human B cell clones can be induced to proliferate and to switch to IgE and IgG_4 synthesis by interleukin 4 and a signal provided by activated $CD4^+$ T cell clones. J Exp Med 1991;173:747-50.
29. Sahoo A, Alekseev A, Tanaka K, Obertas L, Lerman B, Haymaker C, et al. Batf is important for IL-4 expression in T follicular helper cells. Nat Commun 2015;6:7997.

30. Xin G, Zander R, Schauder DM, Chen Y, Weinstein JS, Drobyski WR, et al. Single-cell RNA sequencing unveils an IL-10–producing helper subset that sustains humoral immunity during persistent infection. Nat Commun 2018;9:5037.
31. He JS, Subramaniam S, Narang V, Srinivasan K, Saunders SP, Carbajo D, et al. IgG_1 memory B cells keep the memory of IgE responses. Nat Commun 2017;8:641.
32. Talay O, Yan D, Brightbill HD, Straney EE, Zhou M, Ladi E, et al. IgE^+ memory B cells and plasma cells generated through a germinal-center pathway. Nat Immunol 2012;13:396-404.
33. Looney TJ, Lee JY, Roskin KM, Hoh RA, King J, Glanville J, et al. Human B-cell isotype switching origins of IgE. J Allergy Clin Immunol 2016;137:579-86.e7.
34. Maehara T, Kaneko N, Perugino CA, Mattoo H, Kers J, Allard-Chamard H, et al. Cytotoxic $CD4^+$ T lymphocytes may induce endothelial cell apoptosis in systemic sclerosis. J Clin Invest 2020;130:2451-64.
35. Allard-Chamard H, Alsufyani F, Kaneko N, Xing K, Perugino C, Mahajan VS, et al. $CD4^+$ CTLs in fibrosing mediastinitis linked to *histoplasma capsulatum*. J Immunol 2021;206:524-30.
36. Morimoto Y, Hirahara K, Kiuchi M, Wada T, Ichikawa T, Kanno T, et al. Amphiregulin-producing pathogenic memory T helper 2 cells instruct eosinophils to secrete osteopontin and facilitate airway fibrosis. Immunity 2018;49:134-50.e6.
37. Michailidou D, Schwartz DM, Mustelin T, Hughes GC. Allergic aspects of IgG_4-related disease: implications for pathogenesis and therapy. Front Immunol 2021; 12:693192.
38. Virkud YV, Kelly RS, Croteau-Chonka DC, Celedon JC, Dahlin A, Avila L, et al. Novel eosinophilic gene expression networks associated with IgE in two distinct asthma populations. Clin Exp Allergy 2018;48:1654-64.
39. Tojima I, Murao T, Nakamura K, Arai H, Shimizu S, Kouzaki H, et al. Increased blood group 2 iinate lymphoid cells are involved in blood eosinophilia and itching in Kimura disease. Authorea 2022. https://doi.org/10.22541/au.164181537.77958556/v1.
40. Oettgen HC, Geha RS. IgE regulation and roles in asthma pathogenesis. J Allergy Clin Immunol 2001;107:429-40.
41. Overed-Sayer C, Rapley L, Mustelin T, Clarke DL. Are mast cells instrumental for fibrotic diseases? Front Pharmacol 2013;4:174.
42. Oriente A, Fedarko NS, Pacocha SE, Huang SK, Lichtenstein LM, Essayan DM. Interleukin-13 modulates collagen homeostasis in human skin and keloid fibroblasts. J Pharmacol Exp Ther 2000;292:988-94.

METHODS

Study populations

This study included 11 patients with KD, 25 patients with IgG_4-related disease (IgG_4-RD), 16 patients with active SjS, and 10 patients with CS. CS is a nonspecific inflammatory disease of the salivary glands linked to sialolithiasis. All patients were followed up between 2010 and 2020 at the Department of Kyushu University Hospital in Japan. Open salivary mandibular gland biopsy samples were obtained from patients with IgG_4-RD, while patients with CS underwent submandibulectomy. Lip biopsy samples were performed in patients with SjS. Samples of enlarged draining lymph nodes and affected salivary glands were obtained via biopsy from patients with KD and IgG_4-RD. IgG_4-RD was diagnosed in accordance with the following criteria: (1) persistent (>3 months) symmetrical swelling of more than 2 lacrimal and major salivary glands; (2) high (>135 mg/dL) serum concentrations of IgG_4; and (3) infiltration of IgG_4-positive plasma cells into tissue (IgG_4^+ cells/IgG^+ cells >40%), as determined by immunostaining. All salivary mandibular glands from patients with IgG_4-RD had histologic features of IgG_4-RD. SjS was diagnosed as previously described.[E1] Each patient exhibited objective evidence of salivary gland involvement on the basis of the presence of subjective xerostomia and a decreased salivary flow rate, abnormal findings on parotid sialography, and focal lymphocytic infiltrates in labial salivary glands. None of the patients had a history of treatment with steroids or other immunosuppressants, or infection with human immunodeficiency virus, hepatitis B virus, or hepatitis C virus; none of the patients had sarcoidosis or evidence of lymphoma at the time of the study. All patients had strong lymphocytic infiltration in these tissues.

Immunohistochemical analysis

Formalin-fixed, paraffin-embedded sections (4 μm thick) were prepared and stained using a conventional avidin–biotin complex technique. Sections were incubated with the following primary antibodies: IgE mouse monoclonal antibodies (clone MHE-18; BioLegend, San Diego, Calif), IgG_4 rabbit monoclonal antibodies (clone EP4420; Abcam, Cambridge, United Kingdom), galectin-10 rabbit polyclonal antibodies (catalog NBP1-87688; Novus Biologicals, Littleton, Colo), and anti-CD163 rabbit monoclonal antibodies (clone EPR19518; Abcam). Tissue sections were incubated with primary antibodies for 2 hours and then incubated with biotinylated anti-mouse and rabbit secondary antibodies (Vector Laboratories, Burlingame, Calif). Mayer hematoxylin was used for counterstaining.

Multicolor immunofluorescence staining

Tissue samples were fixed in formalin, embedded in paraffin, and sectioned to a thickness of 4 μm. Specimens were incubated with primary antibodies specific for the following proteins: CD4 (clone EPR6855; Abcam), CD8 (catalog ab4055; Abcam), granzyme A (clone EPR20161; Abcam), GATA3 (clone CM405A; Biocare, Pacheco, Calif), CD19 (clone CM310 A, B; Biocare), Bcl6 (clone CM410A, C; Biocare), CXCR5 (clone MAB190; R&D Systems, Minneapolis, Minn), ICOS (89601; Cell Signaling Technology, Danvers, Mass), IgG_4 (ab109493; Abcam), caspase-3 (9664; Cell Signaling Technology), SLAMF7 (HPA055945; Sigma-Aldrich, St Louis, Mo), RORγ (ab212496; Abcam), Foxp3 (98377; Cell Signaling Technology), Siglec-8 (NBP1-31141; Novus), OPN (clone 1B20; Novus), amphiregulin (bs-3847R; Bioss, Woburn, Mass), IL-4 (clone MAB304; R&D Systems), IL-5 (LS-B7417; LSBio, Seattle, Wash), IL-13 (LS-C104699; LSBio), c-kit (clone LS-A9389; LSBio), and IgE (clone MHE-18; BioLegend). Specimens were then incubated with secondary antibody using an Opal Multiplex Kit (PerkinElmer, Waltham, Mass). The samples were mounted with ProLong Diamond Antifade mountant containing DAPI (Invitrogen; Thermo Fisher Scientific, Waltham, Mass).

Microscopy and quantitative analysis

Images of tissue specimens were acquired using the TissueFAXS platform (TissueGnostics). For quantitative analysis, the entire tissue area was acquired as digital gray-scale images in 5 channels with filter settings for fluorescein isothiocyanate (FITC), Cy3, Cy5, and DAPI. Cells of a particular phenotype were identified and quantified by TissueGnostics's TissueQuest software, with cutoff values determined relative to positive controls. This microscopy-based multicolor tissue cytometry software permits multicolor analysis of single cells within tissue sections in a manner similar to flow cytometry. The principle of the method and the algorithms used have been described in detail elsewhere.[E2]

Flow cytometry and cell sorting

Frozen peripheral blood mononuclear cells were thawed and washed in Dulbecco PBS without calcium and magnesium. Before antibody staining, Fc receptors were blocked using human FcR Blocking Reagent (catalog 130-059-901; Miltenyi Biotec, San Diego, Calif) at a dilution of 1:20 on ice for 15 minutes. Cells were stained for 20 minutes on ice (in the dark) at a concentration of 1×10^4 cells/μL using the following antibody panel: anti-human CD183 (CXCR3)-phycoerythrin (PE)/Cy7 (clone G025H7; BioLegend, 1:20 dilution), anti-human CD196 (CCR6)-APC/Cy7 (clone G034E3; BioLegend, 1:20 dilution), anti-human CD4-APC (clone OKT4; BioLegend, 1:20 dilution), anti-human CD185 (CXCR5)-PE (clone J252D4; BioLegend, 1:20 dilution), anti-human CD279 (PD-1)-FITC (clone EH12.2H7; BioLegend, 1:20 dilution), anti-human CD27-PE (clone M-T271; BioLegend, 1:20 dilution), and anti-human CD62L-FITC (clone DREG-56; BioLegend, 1:20 dilution). Cells were washed with Dulbecco PBS without calcium and magnesium after staining, centrifuged, and resuspended in Flow Cytometry Staining Buffer. Cells were stained with propidium iodide solution (catalog 421301; BioLegend); samples were immediately analyzed and sorted (via FACSVers and FACSAria II, respectively; BD Biosciences, San Jose, Calif). FACS files were analyzed by FlowJo v10 software (Treestar, Ashland, Ore). For bulk RNA-Seq, isolated RNA was immediately processed using reverse transcriptase PCR.

T-cell receptor repertoire analysis from blood samples

Next-generation sequencing–based T-cell receptor repertoire analysis of circulating $CD4^+CXCR5^+$ Tfh cells and circulating $CD4^+CXCR5^-CXCR3^-CCR6^-$ T_H2 cells from a patient with KD and 2 patients with IgG_4-RD, as well as circulating $CD4^+CD27^-CD62L^-$ effector memory T (T_{EM}) cells from a healthy control, was performed by Repertoire Genesis software (Osaka, Japan). The gating strategies for circulating T_H2, Tfh, and T_{EM} are shown in Fig E7. Sequence reads with identical TRV, TRJ, and deduced CDR3 amino acid sequences were defined as unique reads. The copy numbers of unique reads were automatically counted by Repertoire Genesis software in each sample and then ranked in order of copy number. Percentage occurrence frequencies of sequence reads with *TRAV, TRAJ, TRBV,* and *TRBJ* genes in total sequence reads were calculated.

Gene expression microarrays

Total RNA was isolated from cTfh ($CD4^+CXCR5^+PD\text{-}1^+$) cells using the RNeasy Micro Kit (Qiagen, Hilden, Germany), in accordance with the manufacturer's instructions. RNA samples were quantified by an ND-1000 spectrophotometer (NanoDrop Technologies, Wilmington, Del), and the quality was confirmed with a 2200 TapeStation (Agilent Technologies, Santa Clara, Calif). cRNA was amplified and labeled using a human Clariom D assay, in accordance with the manufacturer's instructions. All hybridized microarrays were scanned using an Affymetrix scanner (Affymetrix, Santa Clara, Calif). Arrays were analyzed using the SST-RMA algorithm in the Affymetrix Expression Console Software.

Tissue preparation and cell sorting

For scRNA-Seq, tissue samples of IgG_4-RD were roughly divided, degraded with enzymes, and manually disrupted into a suspension by processing through

a 100 μm strainer with a syringe plunger. $CD3^+$ T cells and $CD19^+$ B cells were prepared from salivary mandibular glands from a patient with IgG_4-RD by positive selection using the EasySep Human CD3 and CD19 Positive Selection Kit II (STEMCELL Technologies, Vancouver, British Columbia, Canada), in accordance with the manufacturer's instructions.

scRNA-Seq of immune repertoires and transcriptomes of infiltrating lymphocytes from affected salivary glands in patients with IgG_4-RD

Single-cell library preparation was carried out with Chromium Next GEM Single Cell 5′ Library & Gel Bead Kit v1.1 (10× Genomics). Cell suspensions were loaded onto a Chromium Single-Cell Chip along with reverse transcription master mix and single-cell 5′ gel beads; the target concentration was 5000 cells per channel. After generation of single-cell gel beads in emulsions, reverse transcription was performed using a Bio-Rad T-100 thermal cycler (Bio-Rad, Hercules, Calif); 16 cycles were used for cDNA amplification. To construct the gene expression library, cDNA was processed in accordance with the protocol for the Chromium Single Cell 5′ Library Construction Kit (10× Genomics), which included 14 amplification cycles. To obtain the B-cell receptor repertoire profile, V(D)J enrichment for B-cell receptors was carried out with Chromium Single Cell V(D)J Enrichment Kit, Human B Cell (10× Genomics). Each cDNA sample was used for V(D)J enrichment with 9 cycles of amplification reaction and library construction, in accordance with the manufacturer's protocol. Libraries were converted with the MGIEasy Universal Library Conversion Kit (MGI Tech, Shenzhen, China) and sequenced on an MGI DNBSEQ-G400 sequencer (MGI Tech) using a 150 pair-end sequencing kit.

Sequencing data analysis

The 10× Genomics Cell Ranger pipeline (v5.0.0) was used to perform sample demultiplexing, alignment to the mm 10 reference genome, barcode/unique molecular identifier, or UMI, processing, and gene counting for each cell. The Seurat packages (v.4.0)[E3] were used for quality checking, filtering, normalization, clustering analyses, and visualization. B-cell receptor repertoire was visualized by Loupe Browser V(D)J 4.0. The quality control data are shown in Fig E8.

Visium spatial gene expression

Spatial transcriptomics analysis was carried out as previously described.[E4-E6]

The Visium Spatial Gene Expression Slide & Reagent Kit (10× Genomics) was used to generate sequencing libraries. Tissue from a patient with IgG_4-RD was cut at a thickness of 10 mm and mounted onto 4 Visium slide-capture areas (6.5 × 6.5 mm).[E4,E5] Sequencing libraries were prepared in accordance with the manufacturer's protocol. After hematoxylin staining of tissue, bright-field images were taken, as described elsewhere for the spatial transcriptomics procedure.[E4,E5] Tissue permeabilization was performed for 15 minutes.

Statistical analysis

GraphPad Prism v8 software (GraphPad Software, La Jolla, Calif) was used for statistical analysis, curve fitting, and linear regression. The Mann-Whitney *U* test, Spearman rank correlations, ANOVA test, and Student *t* test were used to calculate *P* values for continuous nonparametric variables. All statistical analyses were performed by JMP Pro v.16 (SAS Institute, Cary, NC). The Kruskal-Wallis test was used to compare more than 1 population. $P < .05$ was considered statistically significant.

REFERENCES

E1. Maehara T, Mattoo H, Ohta M, Mahajan VS, Moriyama M, Yamauchi M, et al. Lesional $CD4^+$ IFN-gamma$^+$ cytotoxic T lymphocytes in IgG_4-related dacryoadenitis and sialoadenitis. Ann Rheum Dis 2017;76:377-85.

E2. Ecker RC, Steiner GE. Microscopy-based multicolor tissue cytometry at the single-cell level. Cytometry A 2004;59:182-90.

E3. Hao Y, Hao S, Andersen-Nissen E, Mauck WM 3rd, Zheng S, Butler A, et al. Integrated analysis of multimodal single-cell data. Cell 2021;184:3573-87.e29.

E4. Jemt A, Salmen F, Lundmark A, Mollbrink A, Fernandez Navarro J, Stahl PL, et al. An automated approach to prepare tissue-derived spatially barcoded RNA-sequencing libraries. Sci Rep 2016;6:37137.

E5. Ståhl PL, Salmén F, Vickovic S, Lundmark A, Navarro JF, Magnusson J, et al. Visualization and analysis of gene expression in tissue sections by spatial transcriptomics. Science 2016;353:78-82.

E6. Carlberg K, Korotkova M, Larsson L, Catrina AI, Stahl PL, Malmstrom V. Exploring inflammatory signatures in arthritic joint biopsies with spatial transcriptomics. Sci Rep 2019;9:18975.

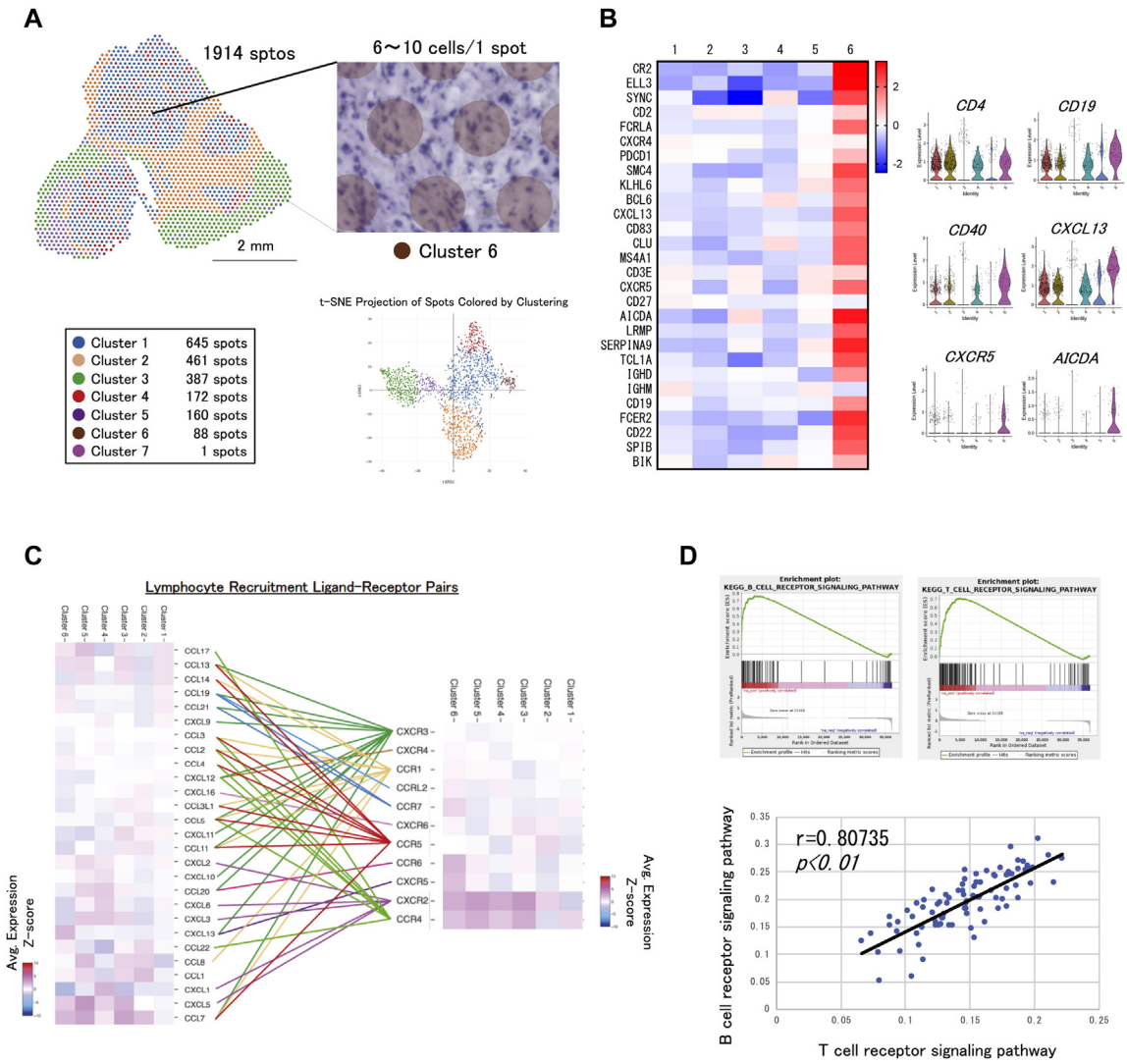

FIG E1. Lesional *AICDA*$^{+}$ *CD19*$^{+}$ B cells revealed by spatial transcriptomics in patients with IgG_4-RD. **A,** Unbiased clustering of spatial transcriptomics spots in a tissue section from a patient with IgG_4-RD. Scale bar, 2 mm. Each spot represents an area from which messenger RNA was captured. *Numbers* and *colors* represent the different clusters that were assigned. For bulk analysis, all spots were selected. Seven clusters were identified across 1914 spots and are shown by t-SNE visualization. **B,** *Left,* Selected gene expression patterns among 6 clusters in the tissue section from a patient with IgG_4-RD. Cluster 7 was removed because of its low spot number. *Right,* Violin plot showing gene expression patterns according to cluster. Cluster 7 was removed because of its low spot number. **C,** *Left, Z*-scored mean log expression heat map of chemokine genes across clusters from Visium data. *Right, Z*-scored mean log expression heat map of chemokine receptor genes across cluster from Visium data. The *colored line* connects matching ligands for each chemokine receptor. **D,** Gene set enrichment analysis (GSEA) performed on $\log_2$ fold changes between gene expression of cluster 6 and the others. GSEA enrichment plot for the 2 significant enriched gene sets: B- and T-cell receptor signaling pathway. The *green* curve represents the running sum of the weighted enrichment score for the gene sets: B-cell receptor signaling pathway (normalized enrichment score [NES] = 1.43; false discovery rate [FDR] *q* value = 0.055) and T-cell receptor signaling pathway (NES = 1.37; FDR *q* value = 0.140). T-cell receptor signaling pathway (n = 88 spots) in cluster 6 correlated with B-cell receptor signaling pathway (n = 88 spots) in cluster 6. The correlation coefficients and *P* values were determined by Spearman rank correlations. **E,** Immunofluorescence staining of AID (*red*), ICOS (*green*), and Bcl6 (*blue*) in B cells in tissues from a patient with IgG_4-RD. *Yellow broken lines* indicate areas within germinal centers; *white lines,* ICOS-expressing T cells and AID-expressing B cells that formed close and extensive intercellular plasma membrane contacts outside germinal centers.

E

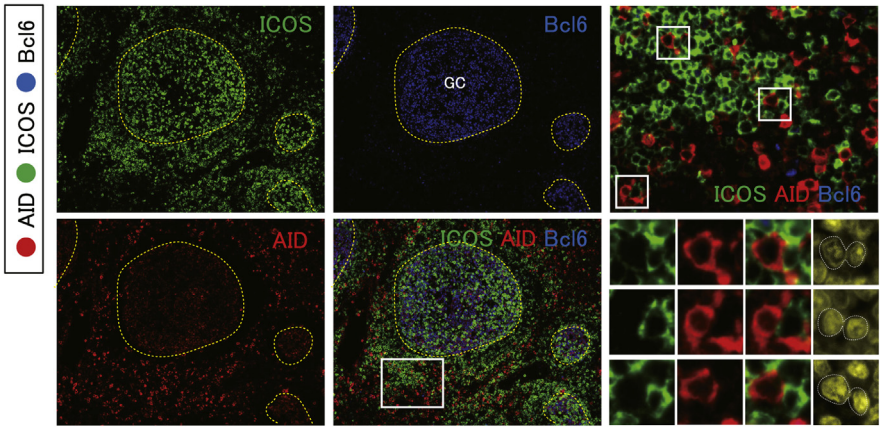

FIG E1. *(Continued).*

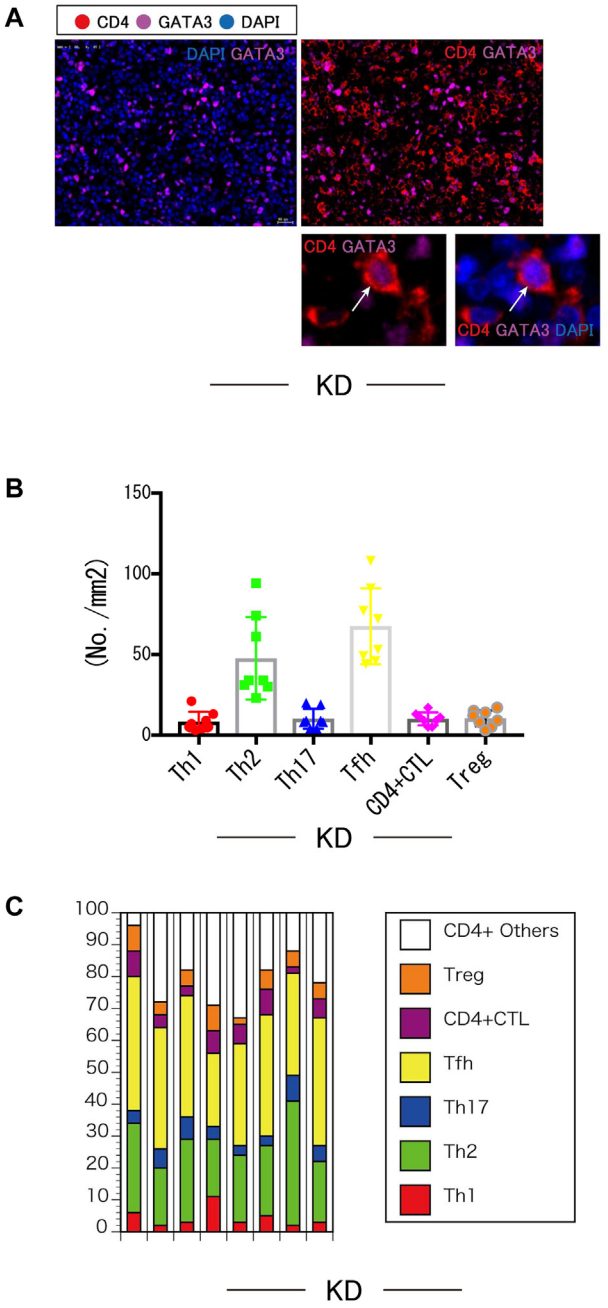

FIG E2. T_H2 and Tfh cells are abundant in patients with KD. **A,** Multicolor immunofluorescence staining of CD4 (*red*), GATA3 (*magenta*), and DAPI (*blue*) in affected tissue from a patient with KD. **B,** Absolute numbers of $CD4^+$T-bet^+ T_H1 cells (*red*), $CD4^+GATA3^+$ T_H2 cells (*green*), $CD4^+ROR\gamma t^+$ T_H17 cells (*blue*), $CD4^+CXCR5^+$ Tfh cells (*yellow*), $CD4^+GZMA^+$ CTLs (*magenta*), and $CD4^+Foxp3^+$ Treg cells (*orange*) in affected tissues from 8 patients with KD. **C,** Relative proportions of $CD4^+$T-bet^+ T_H1 cells (*red*), $CD4^+GATA3^+$ T_H2 cells (*green*), $CD4^+ROR\gamma t^+$ T_H17 cells (*blue*), $CD4^+CXCR5^+$ Tfh cells (*yellow*), $CD4^+GZMA^+$ CTLs (*magenta*), $CD4^+Foxp3^+$ Treg cells (*orange*), and $CD4^+$ Other cells (*white*) in affected tissues from 8 patients with KD.

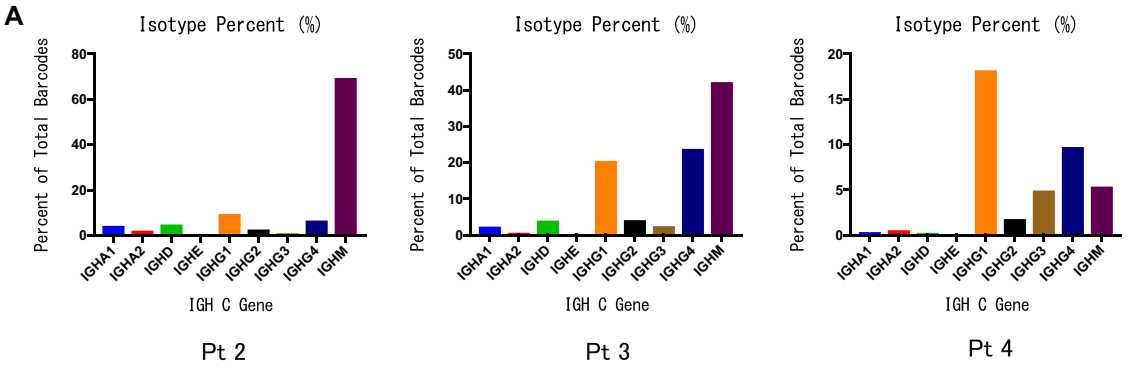

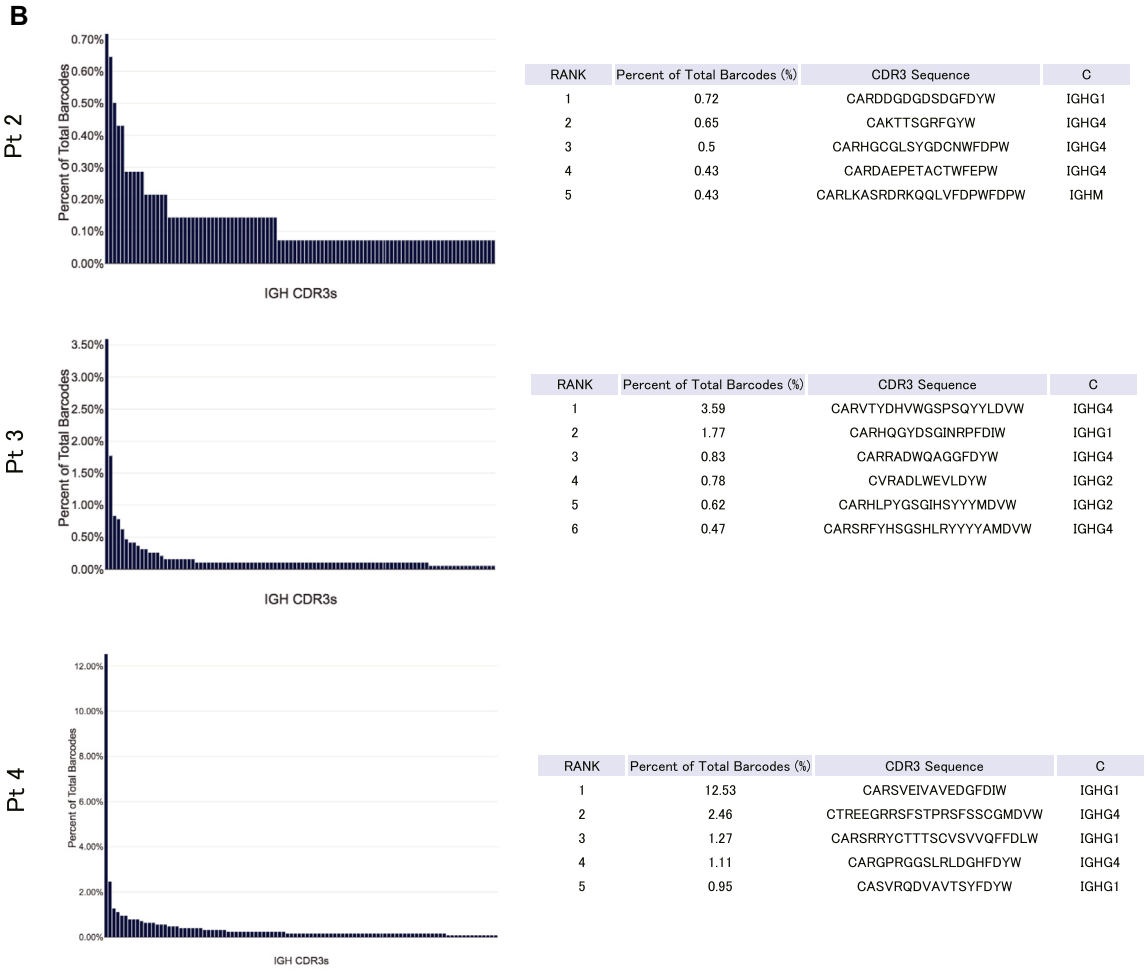

RANK	Percent of Total Barcodes (%)	CDR3 Sequence	C
1	0.72	CARDDGDGDSDGFDYW	IGHG1
2	0.65	CAKTTSGRFGYW	IGHG4
3	0.5	CARHGCGLSYGDCNWFDPW	IGHG4
4	0.43	CARDAEPETACTWFEPW	IGHG4
5	0.43	CARLKASRDRKQQLVFDPWFDPW	IGHM

RANK	Percent of Total Barcodes (%)	CDR3 Sequence	C
1	3.59	CARVTYDHVWGSPSQYYLDVW	IGHG4
2	1.77	CARHQGYDSGINRPFDIW	IGHG1
3	0.83	CARRADWQAGGFDYW	IGHG4
4	0.78	CVRADLWEVLDYW	IGHG2
5	0.62	CARHLPYGSGIHSYYYMDVW	IGHG2
6	0.47	CARSRFYHSGSHLRYYYYAMDVW	IGHG4

RANK	Percent of Total Barcodes (%)	CDR3 Sequence	C
1	12.53	CARSVEIVAVEDGFDIW	IGHG1
2	2.46	CTREEGRRSFSTPRSFSSCGMDVW	IGHG4
3	1.27	CARSRRYCTTTSCVSVVQFFDLW	IGHG1
4	1.11	CARGPRGGSLRLDGHFDYW	IGHG4
5	0.95	CASVRQDVAVTSYFDYW	IGHG1

FIG E3. BCR repertoire of tissue infiltrating T cells in IgG_4-RD patients. **A,** Isotype percentage of immunoglobulin heavy chain (IGH) in B cells from 3 patients with IgG_4-RD (patients 2-4) from scRNA-Seq and B-cell receptor profiling, using 10× Genomics Loupe V(D)J Browser. **B,** IGH CDR3 abundance shows the most frequent clonotypes, from most to least abundant. *Y-axis* shows barcode frequency; *x-axis,* IGH CDR3 sequences; and *inlay,* corresponding CDR3 sequences ordered by frequency, as seen on CDR3 abundance (patients 2-4).

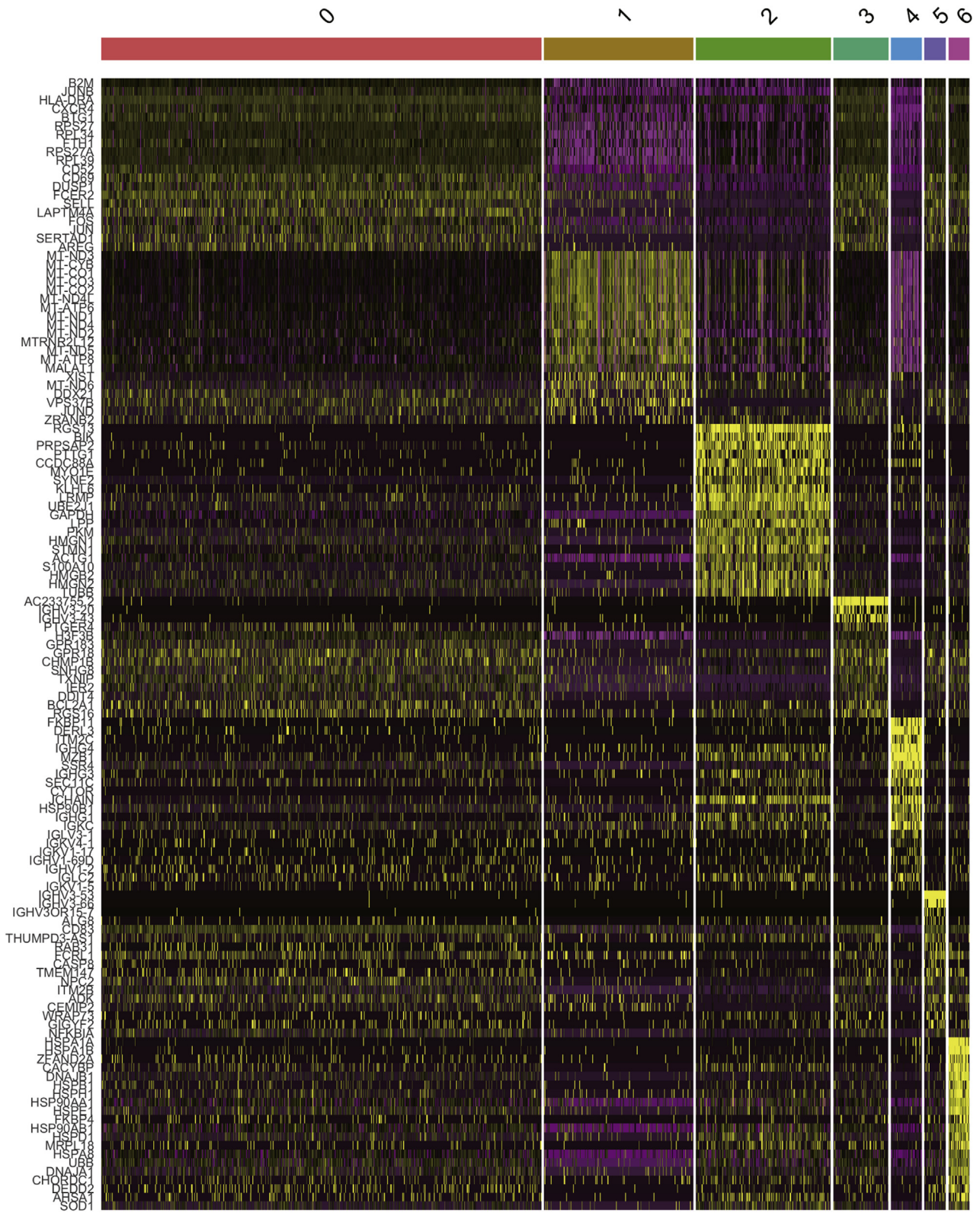

FIG E4. Heat map of the top 10 expressed genes among each cluster using single-cell RNA-Seq. Listed are the top 10 expressed genes among the 7 clusters in a patient with IgG_4-RD (patient 3).

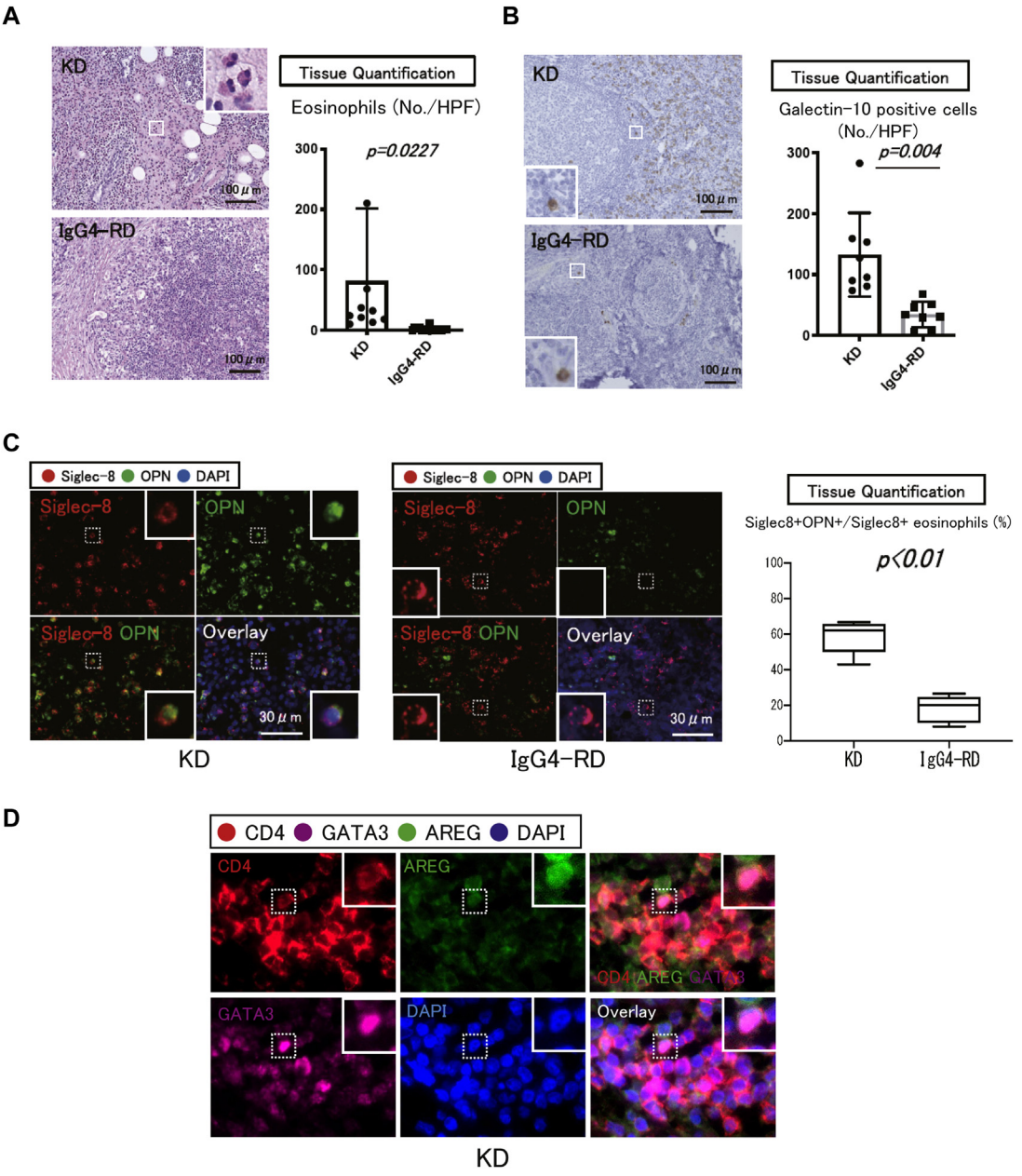

FIG E5. Type 2 immunity–related cells are abundant in patients with KD. **A,** Hematoxylin and eosin staining in affected tissues from a patient with KD and a patient with IgG_4-RD. Numbers of eosinophils were counted per hpf (×400) from 5 different areas in affected tissues from 9 patients with KD and 18 patients with IgG_4-RD. Histologic examination revealed low-level (no./hpf) eosinophilic infiltration in affected tissues. *P* value was determined by Student *t* test. Scale bars, 100 μm. **B,** Staining with galectin-10 (*brown*) monoclonal antibody in affected tissues from a patient with KD and a patient with IgG_4-RD. Counterstaining was performed with Mayer hematoxylin (*blue*). Numbers of galectin-10–positive cells were counted per hpf (×400) from 5 different areas in affected tissues from 8 patients with KD and 8 patients with IgG_4-RD. *P* value was determined by Student *t* test. Scale bars, 100 μm. **C,** Immunofluorescence staining of Siglec-8 (*red*), OPN (*green*), and DAPI (*blue*) in tissues from a patient with KD and a patient with IgG_4-RD. Quantification of Siglec-8^+OPN^+ cells in affected tissues from patients with KD (n = 7) and patients with IgG_4-RD (n = 7). *P* value was determined by Student *t* test. **D,** Multicolor immunofluorescence staining of CD4 (*red*), amphiregulin (AREG) (*green*), and DAPI (*blue*) in affected tissue from a patient with KD. **E,** Absolute numbers of IL-4^+IgE^+c-kit^+ mast cells, IL-5^+IgE^+c-kit^+ mast cells, and IL-13^+IgE^+c-kit^+ mast cells in affected tissues from patients with KD (n = 8) and IgG_4-RD (n = 12).

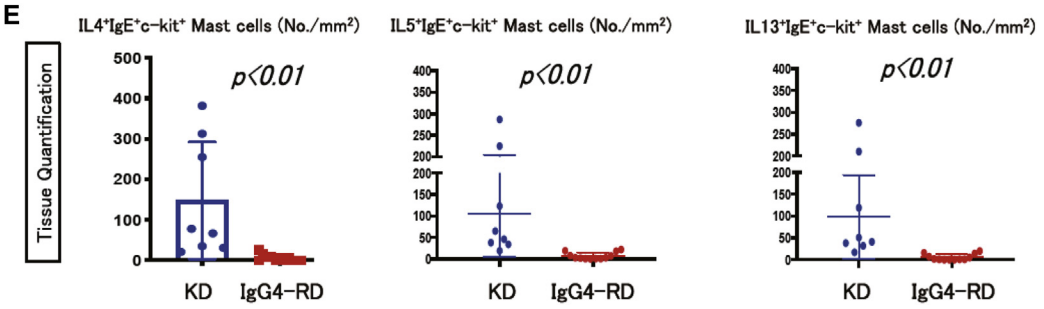

FIG E5. *(Continued).*

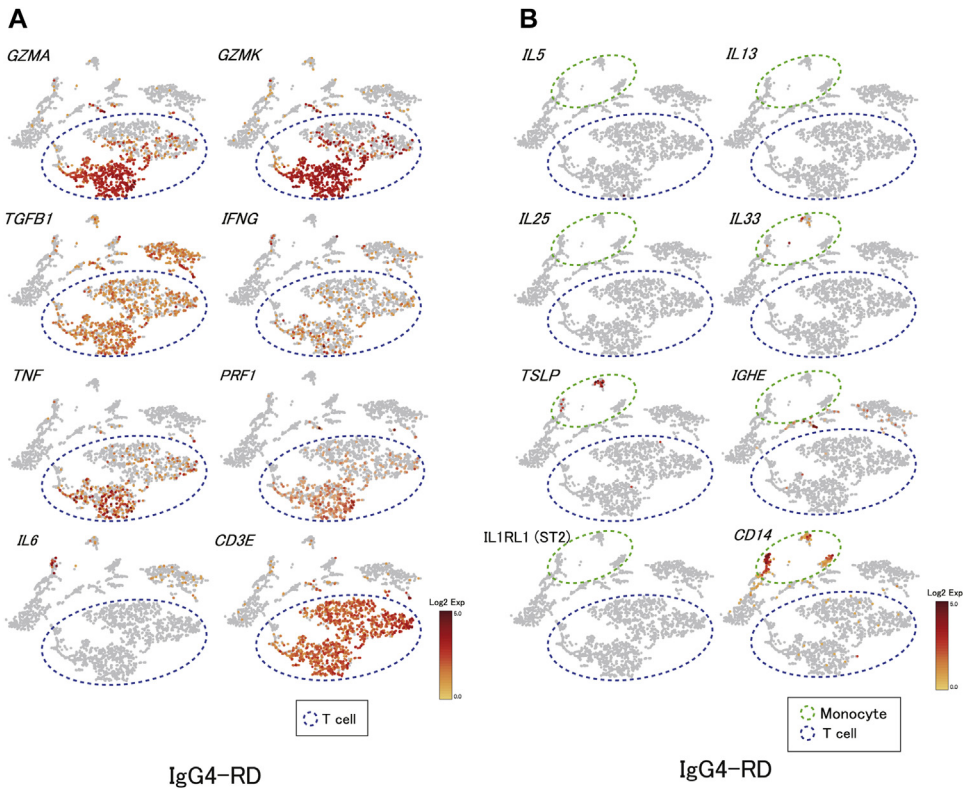

FIG E6. Inflammatory-related cytokines and type 2 immunity–related cytokines in IgG_4-RD. **A,** scRNA-Seq analysis of tissue-infiltrating cells in salivary glands from a patient with IgG_4-RD (patient 1). t-SNE feature plot of selected inflammatory- and cytotoxic-related genes (*GZMA, GZMK, IFNG, TGFB1, TNF, PRF1,* and *IL6*) and *CD3E*. **B,** scRNA-Seq analysis of tissue-infiltrating cells in salivary glands from a patient with IgG_4-RD (patient 1). t-SNE feature plot of type 2 immunity–related genes (*IL5, IL13, IL25, IL33, TSLP, IGHE,* and *IL1RL1*) and *CD14*.

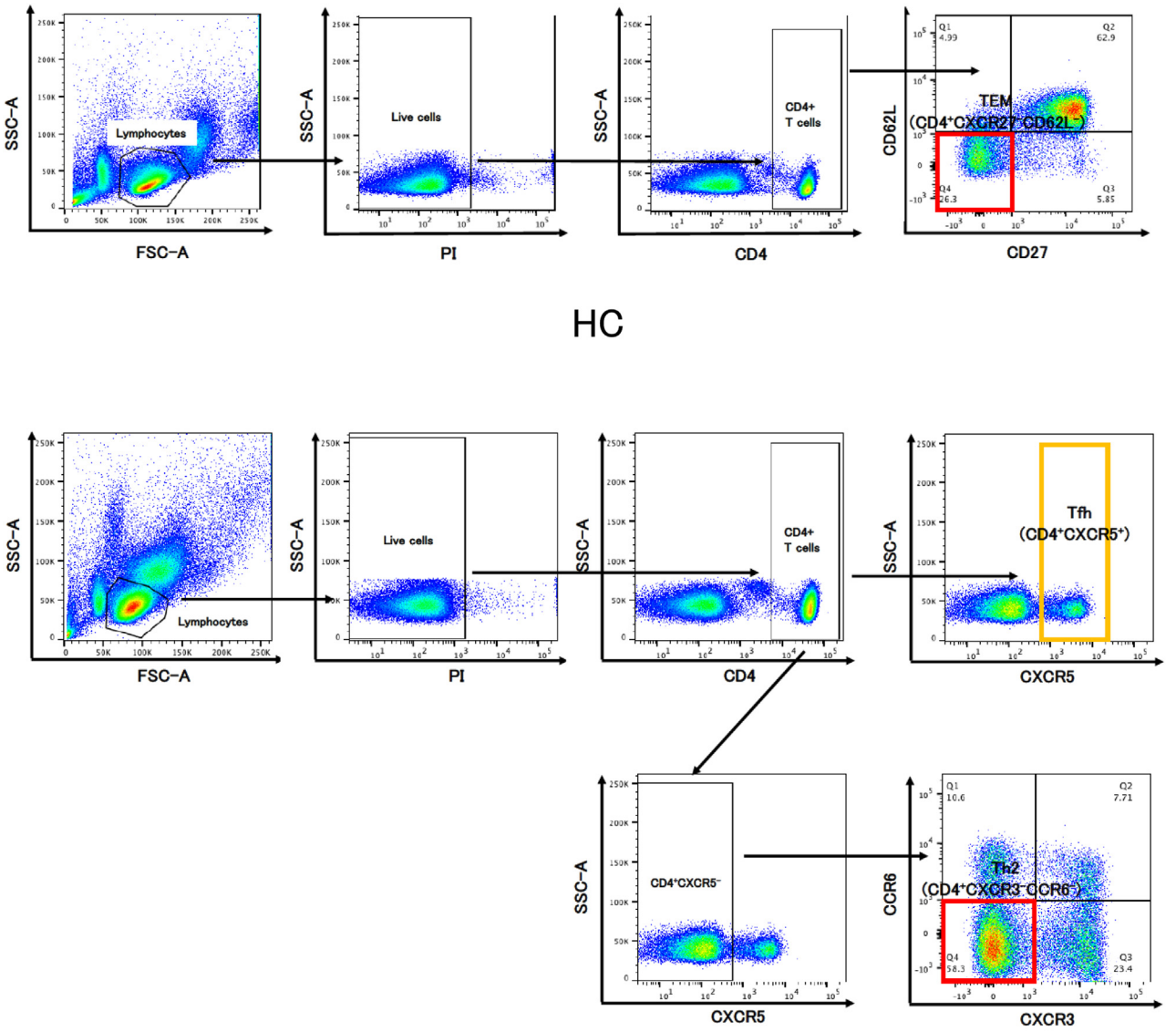

FIG E7. Comprehensive gating strategy used for flow cytometry blood studies from a representative KD patient and control sample.

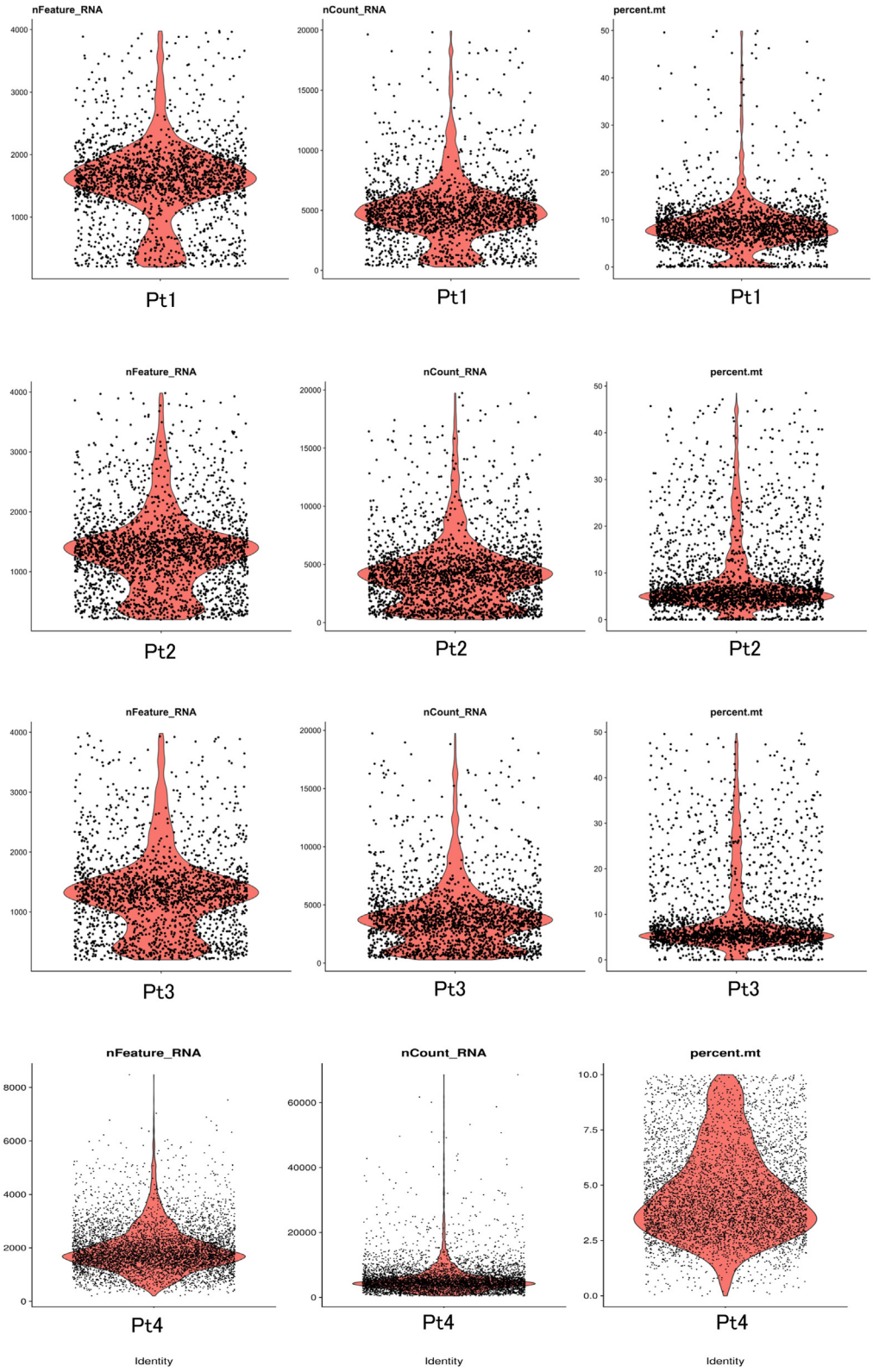

FIG E8. Quality control data for scRNA-Seq. The cells of unique feature counts over 8000-4000, or less than 200 were filtered. Cells with >50-10% mitochondrial counts were filtered (patients 1-4).

TABLE E1. Backgrounds, clinical findings, and serologic findings of 11 KD patients whose affected salivary gland biopsy samples were analyzed in *ex vivo in situ* immunofluorescence studies

Background			Clinical finding		Serologic finding												
Patient no.	Age (years)	Sex	Swelling lesions	Allergy	WBC (/μL)	BASO (%)	LYMP (%)	MONO (%)	NEUT (%)	EOS (%)	EOS count	IgA (mg/dL)	IgE (IU/mL)	IgG (mg/dL)	IgG_4 (mg/dL)	IgM (mg/dL)	CRP (mg/dL)
1	56	M	PG		6860	0.9	19.8	4.8	43.2	29.5	2023	237	14834	1039	96.8	66	0.02
2	16	M	PG	−	7710	1.2	30.3	2.9	23	40	3064	285	9168	1040	ND	113	0.02
3	19	M	PG	Atopic dermatitis	7970	1.3	20.9	3.4	40.1	31.3	2494	ND	10121	ND	ND	ND	0.06
4	41	M	PG, PA, SN	−	8030	0.6	17.9	3.9	25.5	52.1	4183	ND	ND	ND	ND	ND	0.04
5	48	F	PA, LN	+	6760	1	37.4	5.8	42.9	12.9	872	ND	2534	ND	103	ND	ND
6	62	M	PA, SN	−	10190	0.7	23.7	5.6	36	34	3464	ND	577	ND	ND	ND	0.15
7	23	M	LN, PG	+	10950	1.5	25	1	23.3	50.5	5529	273	1854	1236	ND	68	0.07
8	64	M	PA, PG, LN	−	6150	0.7	20.2	5.4	46.7	27	1660	ND	ND	ND	ND	ND	0.02
9	65	M	LN, PG, PA	−	10450	0.4	15.6	4.4	50.1	29.5	3082	ND	34	ND	ND	ND	0.53
10	62	M	LN	−	7700	3	24.3	4.4	53.5	14.8	1139	348	ND	1107	105	37	0.03
11	29	M	SN	+	6790	0.7	27.8	4	55.9	11.6	787	ND	987	ND	ND	ND	0.02

BASO, Basophils; *CRP,* C-reactive protein; *EOS,* eosinophils; *LN,* lymph node; *LYMP,* lymphocytes; *MONO,* monocytes; *ND,* not done; *NEUT,* neutrophils; *PA,* posterior auricle; *PG,* parotid gland; *SN,* skin; *WBC,* white blood cell count.

TABLE E2. Backgrounds, clinical findings, and serologic findings of 25 IgG_4-RD patients whose affected salivary gland biopsy samples were analyzed in *ex vivo in situ* immunofluorescence studies

Background			Clinical finding		Serologic finding								Histologic finding	
Patient no.	Age (years)	Sex	Other swelling lesions	No. of affected organs	SjS ± A/Ro	SjS ± B/La	IgG (mg/dL)	IgG_4 (mg/dL)	IgE (IU/mL)	CRP (mg/dL)	RhF (IU/mL)	ANA	Lymphocytic infiltration*	IgG_4/IgG (CD138)
1	78	M	SMG, PC, LG, LN, PL, BD, RF, KN, AA	9	−	−	4217	524	29	0.55	4	40	3+	50
2	68	F	SMG, LG, LN, PS	3	−	−	2219	152	713	1.19	4	±	3+	75
3	65	F	SMG	1	−	−	1614	192	52	0.16	<5	−	3+	60
4	67	M	SMG	1	−	−	2619	1130	ND	0.14	5	ND	2+	60
5	72	M	SMG	1	−	−	1476	335	38	0.03	3	80	3+	42
6	77	M	SMG, PC, PG, LN, PL, AA, TG	7	−	−	3498	1910	590	0.8	3	±	3+	70
7	76	M	SMG	1	−	−	1954	793	ND	0.02	ND	ND	3+	70
8	41	M	SMG	1	−	−	2736	931	770	0.07	ND	−	3+	60
9	82	F	SMG	1	−	−	2381	823	ND	ND	ND	160	3+	60
10	74	M	SMG, LG, LN, PC	4	−	−	2247	835	627	0.03	6	−	2+	80
11	55	M	SMG	1	−	−	2092	510	ND	0.11	ND	−	3+	70
12	64	M	SMG, LG, LN, PS	4	−	−	2052	748	645	0.09	22	±	3+	50
13	76	M	SMG, OM	2	−	−	1620	157	257	0.45	ND	ND	3+	70
14	74	M	SMG	1	−	−	5646	2140	69	0.38	3	40	3+	80
15	72	F	SMG, LG, LN, PC, KN, SP	6	−	−	6758	1500	13	0.09	8	160	3+	62
16	66	M	SMG, LG, LN, PL, RF, KN	6	−	−	5674	1090	349	1.28	8	±	3+	62
17	61	M	SMG, LG	2	−	−	4970	773	706	0.05	ND	±	3+	70
18	44	M	SMG, LG, LN	3	−	−	1366	188	1619	0.05	5	−	3+	90
19	72	M	SMG, LG	2	−	−	1662	458	603	0.13	ND	±	2+	61
20	52	F	SMG, LG	2	−	−	1317	318	20	0.07	7	−	3+	50
21	54	F	SMG, LN, PL	3	ND	ND	3198	1320	ND	1.62	80	−	3+	60
22	57	M	SMG, LN, PG, PGD, IP	5	−	−	1359	180	460	1.68	16	±	3+	40
23	65	F	SMG	1	−	−	1506	201	ND	0.06	<5	320	3+	80
24	73	M	SMG, LN, PG, AA	4	−	−	1852	708	298	0.04	5	±	3+	84
25	62	F	SMG	1	−	−	1821	256	ND	ND	<5	−	3+	70

AA, Aorta abdominalis; *ANA*, antinuclear antibody; *BD,* bile duct; *CRP,* C-reactive protein; *KN,* kidney; *LG,* lacrimal gland; *LN,* lymph node; *ND,* not done; *OM,* orbital muscle; *PC,* pancreas; *PG,* parotid gland; *PGD,* pituitary gland; *PL,* pleura; *PS,* prostate; *RF,* retroperitoneal fibrosis; *RhF*, rheumatoid factor; *SG,* salivary gland; *SMG,* salivary mandibular gland; *SP,* spleen; *TG,* thyroid gland.

*Greenspan histologic grade.

TABLE E3. Serologic findings of 11 patients with KD and 25 patients with IgG_4-RD

Finding	KD	IgG_4-RD
Serum IgG (normal value, <1747 mg/dL)	1106 ± 93	3208 ± 2105
Serum IgE (normal value, <240 IU/mL)	4284 ± 5579	344 ± 272
Serum IgG_4 (normal value, <121 mg/dL)	98 ± 6	338 ± 264
Eosinophils (normal value, <4%)	30.3 ± 13.8	6.5 ± 4.9
Eosinophil count (no./μL)	2573 ± 1480	412 ± 471

TABLE E4. Differences in ectopic germinal center formation among subjects with KD, IgG_4-RD, SjS, and CS

Disease	Frequency	No./hpf
KD	7/11 (63.6%)	1.7 ± 1.3
IgG_4-RD	18/25 (72%)	1.6 ± 1.2
SjS	2/17 (11.8%)	0.1 ± 0.3
CS	0/5 (0)	0

TABLE E5. Backgrounds, clinical findings, and serologic findings of 4 IgG_4-RD patients whose affected salivary gland biopsy samples were analyzed in scRNA-Seq studies

Background			Clinical finding		Serologic finding								Histologic finding	
Patient no.	Age (years)	Sex	Other swelling lesions	No. of affected organs	SjS-A/Ro	SjS-B/La	IgG (mg/dL)	IgG_4 (mg/dL)	IgE (IU/mL)	CRP (mg/dL)	RhF (IU/mL)	ANA	Lymphocytic infiltration*	IgG_4/IgG (%)
1	73	M	SMG, LN, PG, AA	4	−	−	1852	708	298	0.04	5	−	3+	84
2	57	M	SMG, LN, PG, PGD, IP	5	−	−	1359	180	460	1.68	16	−	3+	40
3	65	F	SMG	1	−	−	1506	201	−	0.06	−	320	3+	80
4	62	F	SMG	1	−	−	1821	256	−	−	−	−	3+	70

AA, Aorta abdominalis; *ANA*, antinuclear antibody; *CRP,* C-reactive protein; *LN,* lymph node; *ND,* not done; *PG,* parotid gland; *PGD,* pituitary gland; *RhF*, rhematoid factor; *SMG,* salivary mandibular gland.

*Greenspan histologic grade.